Genome-wide *in vivo* CRISPR screens identify GATOR1 as a potent tumor suppressor and its loss sensitizes MYC-driven lymphomas to mTOR inhibition

Margaret A. Potts[1,2,3^], Shinsuke Mizutani[1,2,4,^], Yexuan Deng[1,2,3,5^], Srimayee Vaidyanathan[6,7,8#], Keziah E. Ting[6,7,8#], Göknur Giner [1,2,3], Shruti Sridhar[9], Yang Liao[1,3,10,11], Sarah Diepstraten[1,2], Andrew J. Kueh[1,2,3,11], Martin Pal[1,2,12], Geraldine Healey[1,4], Lin Tai[1,4], Zilu Wang[1,2], Christina Konig[1,3], Deeksha Kaloni[1,2], Lauren Whelan[1], Michael Milevskiy[1,2], Giovanna Pomilio[1,6], Andrew H. Wei[1,6], Jane E. Visvader[1,2], Anthony T. Papenfuss[1,2], Stephen Wilcox[1,2], Anand D. Jeyasekharan[9], Wei Shi[1,3,10,11], Emily J. Lelliott[1,2,3,11], Gemma L. Kelly[1,2], Kristin K. Brown[6,7,8*], Andreas Strasser[1,2,*], Marco J. Herold[1,2,3,11*]

[1] The Walter and Eliza Hall Institute of Medical Research, Parkville, Australia

[2] Department of Medical Biology, University of Melbourne, Melbourne, Australia

[3] Olivia Newton-John Cancer Research Institute, Heidelberg, Victoria, Australia

[4] current affiliation: Division of Hematology and Oncology, Department of Medicine, Kyoto Prefectural University of Medicine, Kyoto, Japan

[5] The State Key Laboratory of Pharmaceutical Biotechnology, School of Life Sciences, Nanjing University, Nanjing, China

[6] Peter MacCallum Cancer Centre, Melbourne, VIC 3000, Australia

[7] Sir Peter MacCallum Department of Oncology, The University of Melbourne, VIC 3010, Australia

[8] Department of Biochemistry and Pharmacology, The University of Melbourne, Melbourne, VIC 3010, Australia

[9] Department of Hematology-Oncology, National University Hospital and Cancer Science Institute of Singapore, National University of Singapore, Singapore, Singapore

[10] School of Computing and Information Systems, The University of Melbourne, Parkville, Victoria, Australia

[11] School of Cancer Medicine, La Trobe University, Heidelberg, Victoria 3084, Australia

[12] current affiliation: School of Dentistry and Medical Sciences, Charles Sturt University, Wagga Wagga, NSW, Australia

[^] These authors contributed equally to this work

[#] These authors contributed equally to this work

[*] These authors share joint senior authorship

Word count: 5,100

Number of Figures: 6

Number of Supplementary Figures: 8

Abstract

Identifying tumor suppressor genes is predicted to inform on the development of novel strategies for cancer therapy. To identify new tumor driving processes we have used a genome-wide CRISPR/Cas9 knockout screen in *Eμ-Myc;Cas9* transgenic hematopoietic stem and progenitor cells *in vivo*. We uncovered that loss of either of the GATOR1 complex components - NPRL3, DEPDC5, NPRL2 - significantly accelerated c-MYC-driven lymphoma development in mice, indeed to an extent comparable to loss of p53. In human lymphomas mutations or low expression of the GATOR1 complex genes were mutually exclusive with defects in p53 and correlated with poor survival outcomes for patients with high MYC-expressing cancers. Lymphomas lacking GATOR1 were highly sensitive to mTOR inhibitors, both *in vitro* and *in vivo*. These findings identify inhibition of mTORC1 as a potent tumor suppressive mechanism in c-MYC-driven lymphomagenesis, and suggest a new avenue for therapeutic intervention in GATOR1-deficient lymphomas through mTOR inhibition.

Statement of Significance

Our *in vivo* CRISPR/Cas9 whole genome knockout screens identified the GATOR1 complex as a potent suppressor in c-MYC-driven lymphomagenesis. GATOR1 deficiency obviates the pressure to lose p53 during c-MYC driven lymphoma development and primes these malignant cells for heightened sensitivity to mTOR inhibition, suggesting a novel therapeutic approach.

Introduction

The activation of oncogenes, such as over-expression of c-MYC, causes diverse stresses in cells during early stages of neoplastic transformation. This can activate tumor suppressive processes, such as those coordinated by p53, that will eliminate the early neoplastic cells, thus preventing the development of malignant disease. The transcription factor p53, which can transcriptionally activate mediators of apoptotic cell death (1-4), cell cycle arrest (5), cell senescence, DNA damage repair, adaptation of cellular metabolism and certain other processes, is mutated in ~50% of human cancers (6-8). It is expected that defects in other tumor suppressors may contribute to tumorigenesis in cancers that express wildtype p53. Here, we conducted an unbiased genome-wide CRISPR/Cas9 knockout screen in primary hematopoietic cells predisposed to developing lymphoma *in vivo* that uncovered highly potent tumor suppressors of c-MYC-driven lymphomagenesis (9). Thus far, *in vivo* CRISPR screens were performed with small boutique libraries, or for genome-wide coverage they used transplantation of cancer cell lines but not primary cells. Since lymphomas in the *Eμ-Myc* transgenic model are monoclonal (10), our screens will identify the most powerful tumor suppressor pathways as each manipulated *Eμ-Myc* transgenic hematopoietic stem/progenitor cell (HSPC), deleted for one gene and transplanted into a recipient mouse, will have to compete with thousands of other manipulated HSPCs resulting in the selection of the strongest hit per recipient mouse. This is demonstrated by the observation that deletion of p53 was the most frequent hit in our screen. Interestingly, we also identified two components of the mTORC1 inhibitory complex GATOR1 amongst the top hits and then revealed the importance of this negative regulator of cell metabolism for tumor suppression, including in human cancers through analysis of human cancer genome databases. Of note, we reveal that lymphomas driven by loss of GATOR1 are highly sensitive to mTOR inhibitors, suggesting a therapeutic strategy for GATOR1-deficient cancers over-expressing MYC.

Results

Genome-wide *in vivo* CRISPR/Cas9 knockout screen identifies components of the GATOR1 complex as novel suppressors of lymphomagenesis

To screen for novel tumor suppressor genes in c-MYC-driven lymphomagenesis, primary hematopoietic stem/progenitor cells (HSPCs) from fetal livers of C57BL/6-Ly5.2 *Eμ-Myc;Cas9* double transgenic mouse embryos were transduced with a pooled whole-genome sgRNA library containing 87,987 sgRNAs targeting 19,150 mouse protein coding genes (4-5 sgRNAs per gene) (11), and then transplanted into lethally irradiated congenic C57BL/6-Ly5.1 recipient mice (Fig. 1A). As a positive control, *Eμ-Myc;Cas9* HSPCs were transduced with a sgRNA targeting mouse *p53* (*sgp53)*, as it is known to substantially accelerate c-MYC-driven lymphomagenesis (12). As a negative control, *Eμ-Myc;Cas9* HSPCs were transduced with a sgRNA targeting the human *BIM* gene (*sgControl*). Recipient mice transplanted with *sgControl* HSPCs

developed lymphoma with a median latency of ~140 days post-transplantation, while those transplanted with *sgp53* HSPCs demonstrated significantly accelerated lymphoma development (median latency of ~25 days) (Fig. 1B), consistent with previous reports (13). Notably, several mice transplanted with sgRNA library-transduced HSPCs developed lymphoma early (median latency ~74 days) (Fig. 1B), indicating that select sgRNAs within the library had led to the deletion of genes involved in the suppression of c-MYC-driven lymphomagenesis. All transplanted mice, regardless of the sgRNA that had been transduced into the donor HSPCs and the time when they developed malignant disease, developed sIg- pre-B or sIg+ B cell lymphoma (Supplementary Fig. S1A-B).

To identify sgRNAs that had accelerated lymphomagenesis, we extracted genomic DNA from the spleens of sgRNA library-transduced HSPCs transplanted mice that had developed lymphoma within 75 days of reconstitution (arbitrary cut-off for accelerated lymphoma chosen; n = 60/113) (Fig. 1B). Genomic DNA was subjected to next generation sequencing (NGS) to identify enriched sgRNAs. The majority of tissue sample used for DNA extraction consisted of malignant lymphoma cells in which we identified a small number of highly enriched sgRNAs. We also detected low read counts of large numbers of sgRNAs collectively targeting >75% of all genes, likely representing sgRNAs present in non-malignant hematopoietic cells within the transplanted mouse (Fig 1C, Supplementary Fig. S2A-D). Of the genes for which no sgRNA was represented, 809 (~4%) are deemed essential according to DepMap and the TCGA (14). Collectively, these data indicate comprehensive gene coverage of the genome-wide library in the transduced HSPCs used for the screen.

Hits from our screen were designated as a sgRNA within the top 4 enriched sgRNAs within a given tumor burdened tissue of a transplanted mouse with accelerated lymphoma (Supplementary Table 1). Amongst the top hits were several known tumor suppressors, the most prominent hit being *p53*, for which four of five sgRNAs in the library were enriched across 14 different lymphomas (Fig. 1D-E). Notably, the screen also identified new candidate tumor suppressor genes, including *Nprl3* (two sgRNAs enriched across 3 lymphomas) and *Depdc5* (one sgRNA enriched in one lymphoma) (Fig. 1c). *Nprl3* and *Depdc5* both encode essential components of the GATOR1 complex, a critical negative regulator of mTORC1 (15), suggesting this pathway may play an important role in suppressing c-MYC-driven lymphomagenesis.

Figure 1

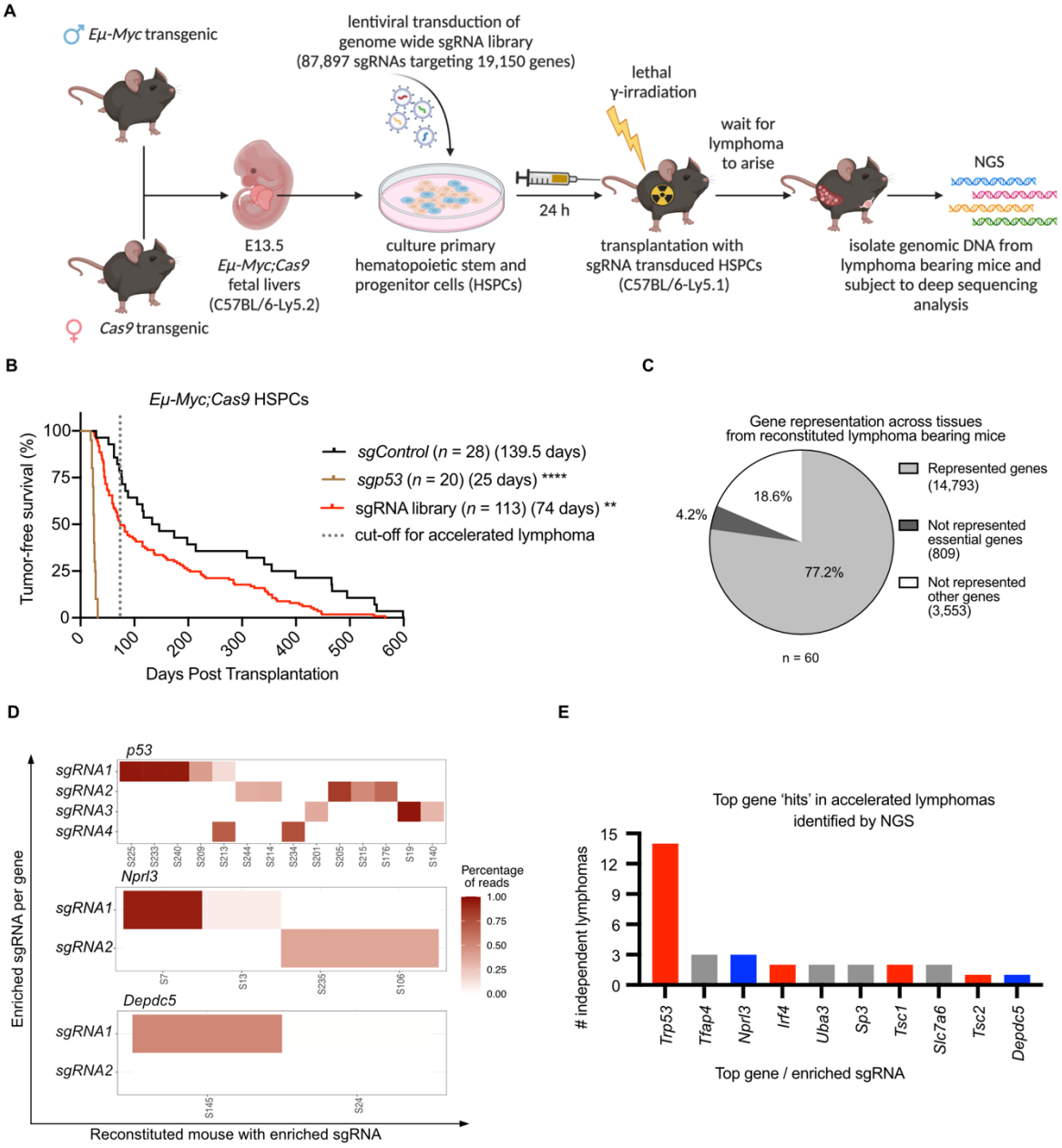
A
♂ Eμ-Myc transgenic
♀ Cas9 transgenic
E13.5
Eμ-Myc;Cas9
fetal livers
(C57BL/6-Ly5.2)
lentiviral transduction of
genome wide sgRNA library
(87,897 sgRNAs targeting 19,150 genes)
culture primary
hematopoietic stem and
progenitor cells (HSPCs)
24 h
lethal
γ-irradiation
transplantation with
sgRNA transduced HSPCs
(C57BL/6-Ly5.1)
wait for
lymphoma
to arise
NGS
isolate genomic DNA from
lymphoma bearing mice and
subject to deep sequencing
analysis
B
Eμ-Myc;Cas9 HSPCs
Tumor-free survival (%)
Days Post Transplantation
sgControl (n = 28) (139.5 days)
sgp53 (n = 20) (25 days) ****
sgRNA library (n = 113) (74 days) **
cut-off for accelerated lymphoma
C
Gene representation across tissues
from reconstituted lymphoma bearing mice
Represented genes
(14,793)
Not represented
essential genes
(809)
Not represented
other genes
(3,553)
18.6%
4.2%
77.2%
n = 60
D
p53
sgRNA1
sgRNA2
sgRNA3
sgRNA4
Nprl3
Depdc5
Percentage
of reads
Enriched sgRNA per gene
Reconstituted mouse with enriched sgRNA
E
Top gene 'hits' in accelerated lymphomas
identified by NGS
independent lymphomas
Trp53
Tfap4
Nprl3
Irf4
Uba3
Sp3
Tsc1
Slc7a6
Tsc2
Depdc5
Top gene / enriched sgRNA

Figure 1. *In vivo* genome-wide CRISPR/Cas9 gene knockout screen identifies novel candidate tumor suppressors.

A, Schematic of the experimental strategy for performing *in vivo* genome-wide sgRNA screens to identify novel tumor suppressors. Fetal liver cells, a rich source of hematopoietic stem/progenitor cells (HSPCs), from E13.5 *Eμ-Myc*;*Cas9* mice (C57BL/6-Ly5.2) were transduced with lentiviruses containing sgRNAs targeting *p53* (*sgp53;* positive control), a negative control sgRNA targeting human *BIM* (*sgControl)* or a whole-genome sgRNA library (11). The transduced HSPCs were injected intravenously (i.v.) into lethally irradiated congenic recipient (C57BL/6-Ly5.1) mice. Lymphoma bearing mice displayed enlarged spleen, lymph nodes and/or thymus. These tissues were harvested and cryopreserved. Genomic DNA was isolated from the spleen, comprising mostly of lymphoma cells but also containing non-transformed hematopoietic cells, and enriched sgRNAs were identified by NGS. **B,** Tumor-free survival of mice transplanted with *Eμ-Myc;Cas9* HSPCs that had been lentivirally transduced with the positive control sgRNA (*sgp53)*, the negative control sgRNA (*sgControl)* or a whole-genome sgRNA library. The dotted line represents cut-off for lymphomas deemed to be accelerated for further analysis. n represents total number of transplanted mice per sgRNA from 6 reconstitution cohorts. Median survival is indicated in brackets. Log-rank (Mantel-Cox) statistical test for survival curve comparison, $^{**}P$=0.0002, $^{****}P < 0.0001$. **C,** DNA sequencing analysis from lymphoma burdened spleens (also containing sgRNAs present in non-malignant cells) from all transplanted mice that were deemed to have shown accelerated lymphoma development (n = 60/113). Of the 19,150 genes targeted by the genome-wide sgRNA library, 77.2% (14,793 genes) were represented by >1 sgRNA, 4.2% (809 genes) were not represented by any sgRNA and are classified as essential genes and 18.5% (3,553 genes) were not represented by any sgRNA but are not essential. **D,** Heatmaps representing top and most frequently enriched sgRNAs per gene identified in lymphoma burdened spleens from mice that had been transplanted with the whole-genome sgRNA library transduced *Eμ-Myc*;*Cas9* HSPCs. *p53* (4/5 sgRNAs, 14 lymphomas), *Nprl3* (2/5 sgRNAs, 4 lymphomas), and *Depdc5* (1/5 sgRNAs, 1 lymphoma). Data are presented as proportion of reads assigned to sgRNA over all reads within a given lymphoma burdened spleen sample. **E,** Top 10 gene hits, determined by frequency of their sgRNA detected in independent lymphomas from mice with accelerated lymphoma onset and being highly enriched (>50% of reads within a lymphoma) by sequencing. Bars in red represent well known tumour suppressor genes; grey and blue bars represent novel tumour suppressor genes.

To validate NPRL3, DEPDC5 as well as NPRL2, the third component of the GATOR1 complex (Fig. 2A), as tumor suppressors, two independent sgRNAs targeting each of their genes were individually introduced into *Eμ-Myc;Cas9* HSPCs that were then transplanted into recipient mice. Strikingly, all sgRNAs targeting *Nprl3*, *Depdc5* or *Nprl2* significantly accelerated c-MYC-driven lymphomagenesis, notably, to a similar

extent as the sg*p53* (Fig. 2B-D, Supplementary Fig. S3A-C). Deletion of *Nprl3*, *Depdc5* and *Nprl2* by CRISPR/Cas9 was confirmed by targeted gene sequencing of gDNA isolated from cell lines derived from these primary lymphomas (Fig. 3E).

To examine if these findings are relevant to human cancer, we analyzed data from The Cancer Genome Atlas (TCGA). This revealed that *GATOR1-low* tumors (defined as those with either *NPRL3*, *DEPDC5* or *NPRL2* gene expression in the bottom quartile) were associated with significantly poorer overall patient survival compared to *GATOR1-high* tumors in Burkitt lymphoma (driven by c-*MYC* chromosomal translocations), and in all *MYC*-high expressing cancers more broadly (Fig. 2F-G). These findings identify the GATOR1 complex as a suppressor of MYC-driven cancers, particularly c-MYC-driven B cell lymphoma.

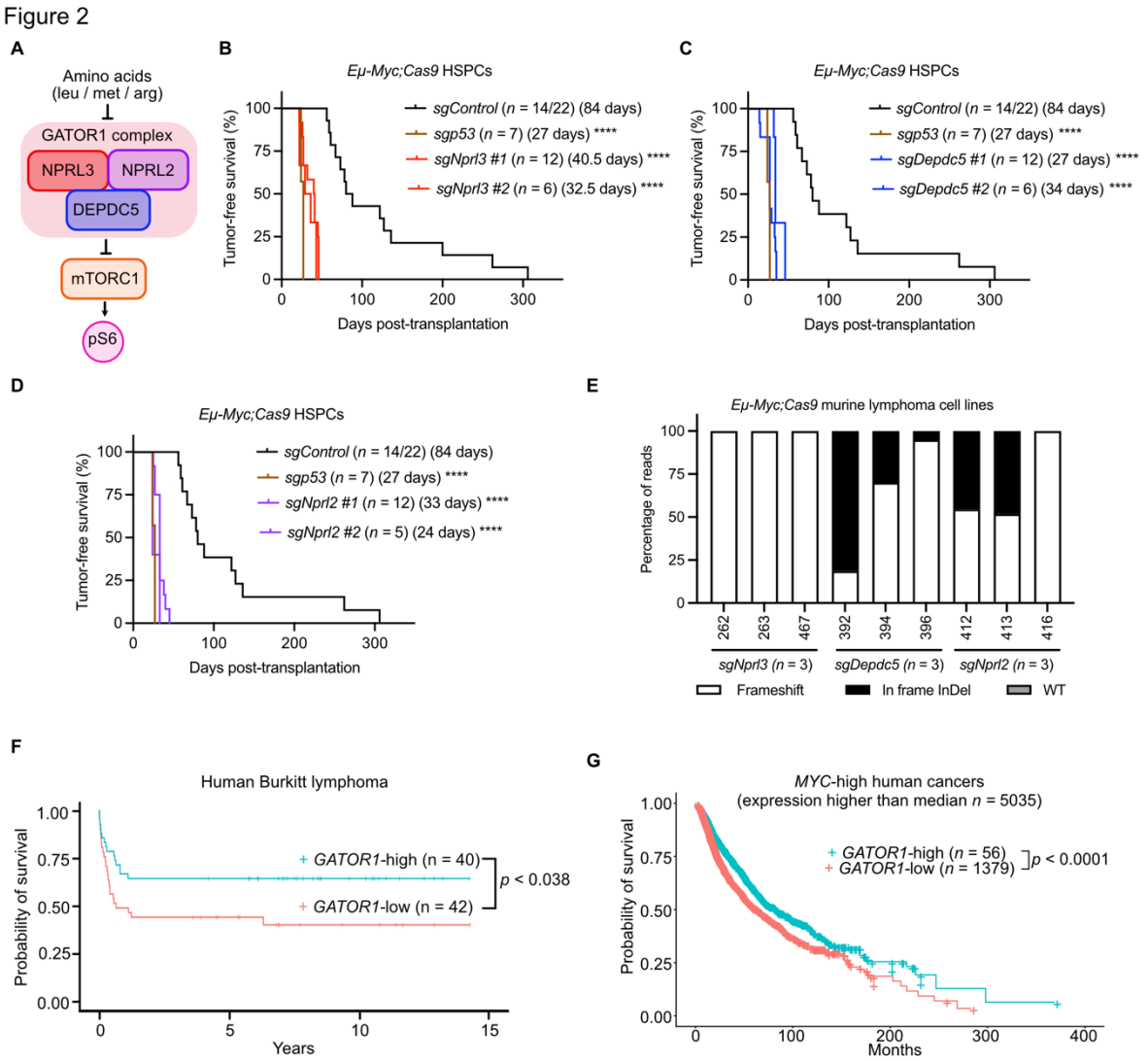

Figure 2. GATOR1 complex components validation as tumor suppressors of MYC driven lymphomagenesis in human MYC-driven cancers.

A, Schematic of the GATOR1 complex, consisting of three proteins, NPRL3, DEPDC5 (both identified as hits in our genome-wide screen), and NPRL2. The GATOR1 complex negatively regulates mTORC1 signaling in response to the availability of the amino acids leucine (leu), methionine (met) and arginine (arg). **B-D,** Tumor-free survival of mice transplanted with *Eμ-Myc;Cas9* HSPCs that had been transduced with either the sg*p53* (positive control), the negative control sgRNA (*sgControl*) or two independent sgRNAs each for targeting either *Nprl3* **B,** *Depdc5* **C,** or *Nprl2* **D**. *n* represents the number of transplanted mice per sgRNA across two transplanted mouse cohorts. Median survival is indicated in brackets. Log-rank (Mantel-Cox) test was used for comparison of mouse survival curves, ****$P < 0.0001$. **E**, Proportions of frameshift, in frame InDels or WT sequence reads per sample for the target gene of each sgRNA, analyzed by next generation sequencing of lymphoma cell lines derived from lymphomas of recipient mice that had

been transplanted with *sgNrpl3, sgDepdc5, sgNprl2* transduced *Eμ-Myc;Cas9* HSPCs. **F**, Probability of survival of human patients with Burkitt lymphoma, a cancer driven by *c-MYC* chromosomal translocations, stratified by *GATOR1* expression, where the *GATOR1*-low (n = 42) strata is defined as expression of either the *NPRL3*, *DEPDC5* or *NPRL2* gene in the lowest quartile. The others were grouped into the *GATOR*1-high strata (n = 40). Kaplan-Meier statistical test, ****P < 0.038. **G,** Human TCGA pan-cancer analysis of *MYC*-high (expression higher than median, n = 5,035 patient samples) tumors, showing the difference in probability of survival between *GATOR1*-low group samples (defined as tumors with *NPRL2* or *DEPDC5* or *NPRL3* expression in the bottom quartile, median survival 47 months, n = 1,379 patient samples) versus *GATOR1*-high group samples (defined as tumors with *NPRL2* and *DEPDC5* and *NPRL3* expression in the top quartile, median survival 70 months, n = 56 patient samples). Kaplan-Meier statistical test, ****P < 0.0001.

Loss of GATOR1 obviates the pressure for p53 mutation in c-MYC-driven lymphomagenesis

Given that deletion of GATOR1 components accelerated lymphomagenesis to a similar extent as p53 deletion, we wondered whether mutations in their genes were mutually exclusive, which may indicate they function within a connected pathway. We examined p53 functionality and mutational status in *sgControl* and GATOR1-deficient lymphomas. Consistent with previous reports (16,17), we found that ~30% of *sgControl* lymphomas had acquired p53 pathway defects, evidenced by increased levels of mutant p53 protein and/or $p19^{ARF}$ (16-18) (Fig. 3A, Supplementary Fig. S4A). In contrast, no such abnormalities were found in GATOR1-deficient lymphomas (Fig. 3A, Supplementary Fig. S4A). To validate these findings, we treated lymphoma cell lines in culture with nutlin-3a, which induces apoptotic death in a p53-dependent manner (19). 3/10 *sgControl* lymphomas were resistant to nutlin-3a, whereas all GATOR1-deficient lymphomas were highly sensitive (n = 27; Fig. 3A, Supplementary Fig. S4B). Next generation sequencing confirmed that the three nutlin-3a-resistant *sgControl* lymphomas had acquired pathologic *p53* mutations, whereas 26/27 (~96%) of GATOR1-deficient lymphomas maintained wild-type *p53* status (Fig. 3A). Extending our analysis to human tumors, we observed mutual exclusivity of mutations in *p53* and GATOR1 complex genes in diffuse large B cell lymphoma samples (DLBCL, n = 73 samples) (Fig. 3B).

Loss of one *p53* allele substantially accelerates tumorigenesis in *Eμ-Myc* mice, and almost all lymphomas arising in such mice are selected for loss of the second *p53* allele (known as loss of heterozygosity, LOH) (17). We examined whether deletion of *Nprl3* or *Depdc5* would obviate the selective pressure to lose p53 function through *p53* LOH in c-MYC-driven lymphomagenesis. To examine this, we transduced $p53^{+/-}$*;Eμ-Myc;Cas9 or* $p53^{-/-}$*;Cas9* HSPCs with sgRNAs targeting *Nprl3, Depdc5* or a control sgRNA and

transplanted these cells into lethally irradiated recipient mice. Remarkably, recipient mice transplanted with *sgNprl3* or *sgDepdc5* transduced *p53*$^{+/-}$*;Eμ-Myc;Cas9* HSPCs developed lymphoma 14 days post-transplantation, significantly faster than mice transplanted with control sgRNA transduced *p53*$^{+/-}$*;Eμ-Myc;Cas9* HSPCs (median tumor latency 35 days) (Fig. 3C). This accelerated lymphoma onset indicated that p53 function was (i) either abrogated by loss of the other *p53* allele or (ii) that GATOR1-deficiency obviated the need for complete loss of p53 function in MYC-driven lymphomagenesis. To discriminate between these two scenarios, we probed the lymphomas for p19^{ARF}, a protein that is increased when p53 function is lost. While 5/6 control lymphomas displayed high levels of p19^{ARF}, this was not seen in any of the lymphomas (n = 0/12) from mice transplanted with *sgNprl3* or *sgDepdc5* transduced *p53*$^{+/}$*;Eμ-Myc;Cas9* HPSCs (Fig. 3D). Notably, GATOR1 deficiency did not significantly accelerate thymic T lymphoma development driven by the absence of p53, as evidenced by transplantation of *sgNprl3* or *sgDepdc5* transduced *p53*$^{-/-}$*;Cas9* HSPCs into lethally irradiated mice (Supplementary Fig. S4C). These findings demonstrate that ablating the function of GATOR1 obviates the need to acquire mutations in *p53* during MYC-driven lymphoma development and when p53 is lost deletion of GATOR1 does not further enhance T lymphoma development.

p53 is not a major transcriptional regulator of the expression of components of the GATOR1 complex

The findings described above may indicate that GATOR1 could function downstream of p53 and is critical for its tumor suppression. Alternatively, GATOR1 and p53 may function in distinct processes for tumor suppression, with ablation of either being sufficient to accelerate MYC-driven lymphoma development. To discriminate between these two possibilities, we examined whether genes for the components of the GATOR1 complex can be activated by p53. We treated isogenic parental p53 WT *Eμ-Myc* lymphoma cells and their *p53* KO derivatives, generated using CRISPR with etoposide to induce DNA damage and thereby activate p53 (8). As anticipated, expression of *Cdkn1a* (p21), a canonical p53 target gene, increased markedly following treatment with etoposide only in the *p53* WT but not the *p53* KO lymphoma cells (Supplementary Fig. S5A-B). After exposure to etoposide, a ~2-fold increase in *Nprl3* mRNA was seen in the *p53* WT lymphoma cells but not in the *p53* KO derivatives (Fig. 3E). An increase in *Depdc5,* but not *Nprl2*, was also observed after etoposide treatment (Supplementary Fig. S5A-B). Similar results were obtained in a murine *HoxA9-Meis1* translocation driven acute myeloid leukemia (AML) cell line as well as in the human BL2 Burkitt lymphoma and human DoHH2 Non-Hodgkin's lymphoma cell lines (Supplementary Fig. S5C-E). To further examine a potential p53 mediated transcriptional regulation of *Nprl3*, we engineered *Nprl3*-IRES-citrine gene expression reporter mice (Fig. 3F) and intercrossed them with *Eμ-Myc* transgenic mice to generate *Nprl3*-IRES-citrine;*Eμ-Myc* reporter lymphoma cell lines. We then measured citrine fluorescence (reporting on *Nprl3* induction) after 6 or 24 h treatment with nutlin-3a

or etoposide to activate p53 and observed a minor, albeit significant, induction of citrine (Fig. 3G). Collectively, these data demonstrate that *Nprl3* can be transcriptionally induced following p53 activation.

To examine whether *Nprl3* is a direct transcriptional target of p53, we re-analyzed published ChIP-sequencing data from γ-irradiated murine B cells. This revealed that p53 binds at the *Nprl3* locus, but not at the *Nprl2* or *Depdc5* loci (Supplementary Fig. S6A; (20)). However, our CUT and RUN analysis showed that in *Eμ-Myc* lymphoma cells p53 binding to the *Nprl3* promoter is only weak (Supplementary Fig. S6B). To explore the role of p53 in regulating *Nprl3* expression further we generated gene-targeted mice in which the *Nprl3* promoter is mutated to disrupt p53 binding without disrupting the binding of other transcription factors in this locus (Supplementary Fig. S6C). Notably, this *Nprl3* promoter mutant (hereafter denoted *NPM*) mouse model produced viable offspring, demonstrating that NPRL3 expression remained adequate for embryonic development (Supplementary Fig. S6D); of note complete loss of NPRL3 causes embryonic lethality (21,22). We hypothesized that if p53 mediates tumor suppression through NPRL3, then mutating its binding motif in the *Nprl3* promoter may accelerate lymphomagenesis in *Eμ-Myc* mice. To test this, we transplanted fetal liver cells from $NPM^{KI/KI}$;*Eμ-Myc* or $NPM^{KI/WT}$;*Eμ-Myc* transgenic and control *Eμ-Myc* littermate mice into lethally irradiated recipient mice and monitored lymphoma development. Notably, the *NPM* mutation did not accelerate lymphoma development (Supplementary Fig. S6E). qRT-PCR analysis demonstrated that *Nprl3* gene expression was still induced in $NPM^{KI/KI}$;*Eμ-Myc* lymphoma cells following treatment with etoposide (Supplementary Fig. S6F). Collectively, these data indicate that the expression of components of the GATOR1 complex is not majorly regulated by p53; i.e. p53 and GATOR1 likely suppress tumorigenesis through distinct processes.

Figure 3

A

Genotype of *Eμ-Myc; Cas9* lymphoma cell line	N cell lines with p53 pathway alterations detected by Western blotting	N cell lines resistant to nutlin-3a	N cell lines with *p53* mutations identified by NGS	*p53* mutations identified by NGS
sgControl	5/14	3/9	3/10	451: Ex4 65bp del. 245: Ex8 R>C 246: Ex8 R>H
sgNprl3	0/12	0/12	0/9	
sgDepdc5	0/12	0/9	0/8	
sgNprl2	-	0/6	1/8	413: Ex8 R>T

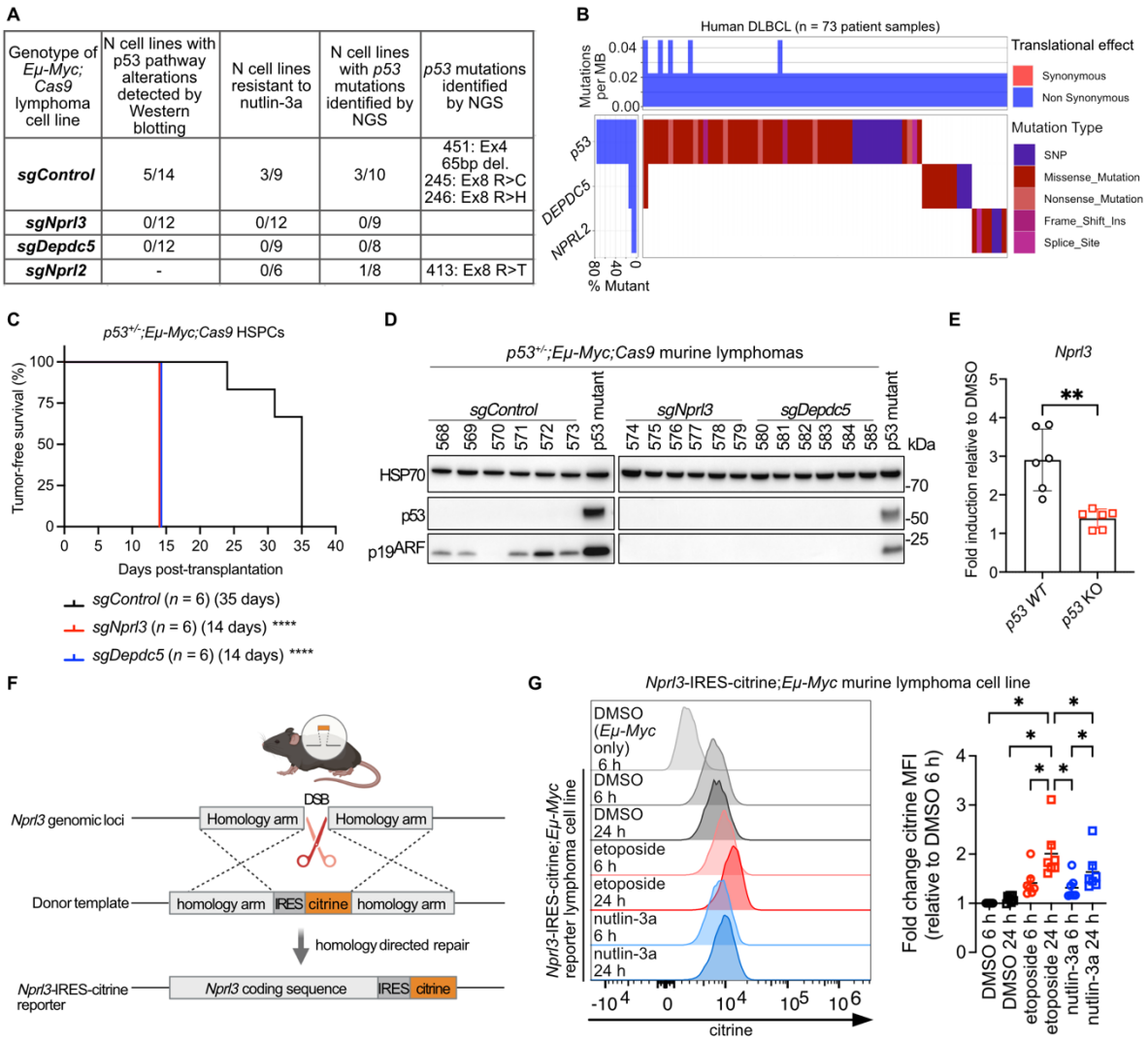

Figure 3. GATOR1-deficiency obviates the pressure to lose p53 function during c-MYC-driven lymphomagenesis.

A, Summary table of *p53* status in *sgControl*, *sgNprl3*, *sgDepdc5* and *sgNprl2* lymphoma cell lines tested through next generation sequencing of exons 4-12 of the *p53* genomic locus to identify mutations. 3/10 *sgControl*, 0/9 *sgNprl3*, 0/8 *sgDepdc5* and 1/8 *sgNprl2* lymphoma cell lines tested carried mutations in the *p53* gene. Note, *sgNprl2* cell line 412 carries a mutation in exon 8 of *p53*. Western blotting to detect stabilized p53 and p19^{ARF} protein; sensitivity to nutlin-3a where defects in p53 function confer profound resistance (19). **B**, Mutational analysis of human diffuse large B cell lymphoma (DLBCL) samples where mutations in *p53* and *DEPDC5* or *NPRL2* are found to be mutually exclusive. $n = 73$ patient samples, $P < 0.0001$ using Fisher's exact test. **C**, Tumor-free survival of mice transplanted with *p53*$^{+/-}$*;Eμ-Myc;Cas9* HSPCs transduced with either a negative control *sgControl*, *sgNprl3* or *sgDepdc5*. n represents the number

of recipient mice per sgRNA in brackets from one reconstitution cohort. Log-rank (Mantel-Cox) statistical test for survival curve comparison, ****$P < 0.0001$. **D**, Western blot analysis to identify *p53* loss of heterozygosity (LOH), as reflected by stabilized high levels of mutant p53 protein or $p19^{ARF}$ protein, from lysates of the spleens of lymphoma burdened recipient mice that had been transplanted with *p53*$^{+/-}$*;Eμ-Myc;Cas9* HSPCs transduced with lentiviruses expressing the negative control sgRNA (*sgControl*; $n = 6$), *sgNprl3* ($n = 6$) or *sgDepdc5* ($n = 6$). Blotting for HSP70 served as a loading control. Molecular weight of proteins is represented in kDa. Cell lysate from a p53 mutant *Eμ-Myc* lymphoma cell line (EMRK1172) (23) served as a positive control for stabilized high levels of mutant p53 protein and $p19^{ARF}$ proteins. **E,** *Nprl3* gene induction following treatment with etoposide (1 μg/mL, 6h) relative to treatment with DMSO (vehicle control) measured by qRT-PCR in isogenic *p53* WT or *p53* knockout (KO) *Eμ-Myc* mouse lymphoma cell lines ($n = 3$ cell lines, 2 independent experiments). Data were normalized to the *Hmbs* housekeeping gene and presented as mean ± SEM. Unpaired, two-tailed Student *t-test*, *$P < 0.05$, **$P < 0.005$. **F,** Schematic representation of the *Nprl3*-IRES-citrine reporter mouse model that was generated through CRISPR/Cas9 homology directed repair using a donor template strand. **G**, *Nprl3-IRES-citrine* reporter mice were inter-crossed with *Eμ-Myc* transgenic mice and lymphoma cell lines were derived from lymphoma bearing *Nprl3-IRES-citrine*;*Eμ-Myc* mice. These lymphoma cell lines were pre-incubated for 30 min with 25 μM of the broad-spectrum caspase inhibitor Q-VD-OPH (to prevent cell demolition due to late stage apoptosis) then treated for 6 h or 24 h with the p53 activating drugs etoposide (1μg/mL), nutlin-3a (10 μM) or DMSO (vehicle control) and citrine expression was measured by flow cytometry. Data are presented as mean ± SEM. Non-parametric One-Way ANOVA with Tukey's multiple comparison, *$P < 0.05$, **$P < 0.005$.

GATOR1 deficiency augments mTORC1 activity and perturbs cellular metabolism

The GATOR1 complex is well established as an inhibitor of mTORC1 (15). We therefore hypothesized that lymphomas deficient in GATOR1 components would exhibit elevated mTORC1 signaling and consequent alterations in cellular metabolism. Indeed, at steady state, we observed substantially higher levels of phosphorylated (i.e. activated) S6, indicative of increased mTORC1 activity, in *Eμ-Myc* lymphoma cells lacking NPRL3 or DEPDC5 compared to control *Eμ-Myc* lymphoma cells (Fig. 4A). To identify changes in mTORC1-regulated metabolic pathways caused by loss of GATOR1 function, we performed RNA sequencing on control and NPRL3 or DEPDC5 deficient lymphoma cells following culture in either full medium (10% fetal calf serum; FCS), or under starvation conditions in medium with only 1% FCS, the latter repressing mTORC1 activity. In both conditions, GATOR1-deficient lymphoma cells displayed elevated expression of genes involved in mTORC1 regulated metabolic pathways, including

lipid/cholesterol biosynthesis, pentose phosphate pathway and one-carbon metabolism (Fig. 4B, Supplementary Fig. S7A-B). This reveals that GATOR1 deficiency promotes constitutive mTORC1 activation and renders cells less sensitive to external factors that repress this pathway. No differences in mitochondrial function were seen when comparing GATOR1-deficient and control lymphoma cells (Supplementary Fig. S8A). However, consistent with known functions of mTORC1 (15), we observed a trend towards elevated *de novo* lipogenesis in GATOR1-deficient lymphoma cells (Supplementary Fig. S8B), as well as increased incorporation of O-propargyl-puromycin (OPP) into nascent proteins, indicative of augmented translation (Fig. 4C, Supplementary Fig. S8C). Other processes commonly subverted in *Eμ-Myc* lymphoma cells, such as apoptosis, were normal in GATOR1-deficient lymphoma cells, given that they were readily killed by treatment with etoposide or the MCL-1 inhibitor S63845 (24) (Supplementary Figure S8D). Additionally, expression of *p53* mRNA and p53 function were comparable between GATOR1-deficient and control lymphoma cells (Supplementary Figure S8E). These findings show that loss of GATOR1 promotes aberrant mTORC1 signaling with consequent reprogramming of cellular metabolism.

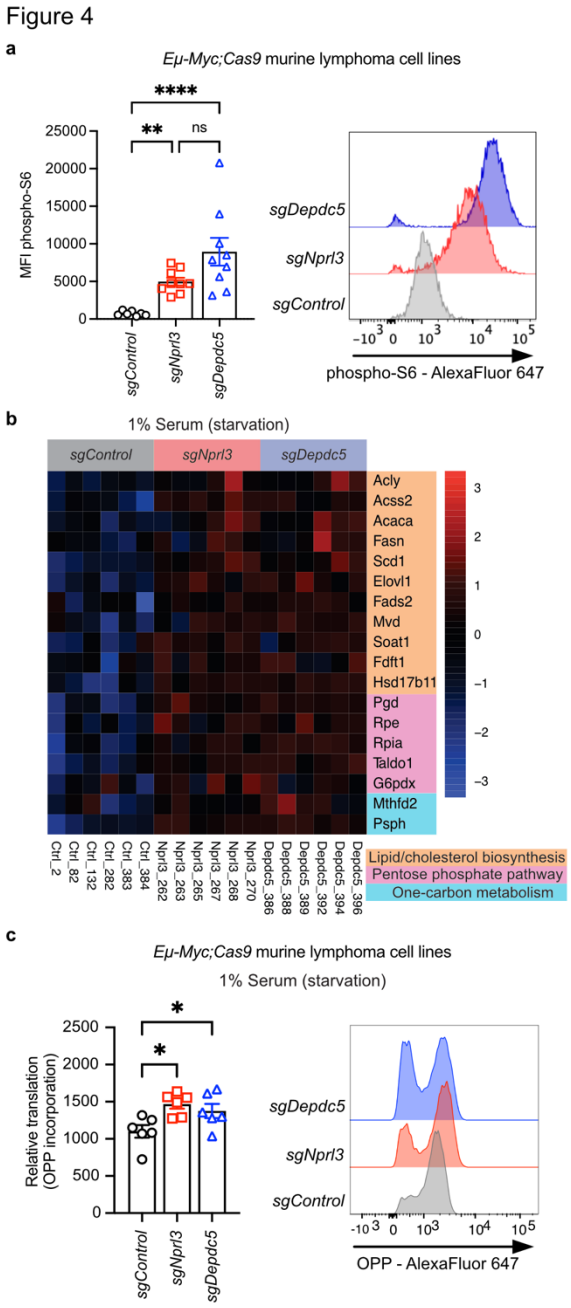

Figure 4. GATOR1-deficient lymphomas display altered mTORC1 regulated metabolic pathways. **A**, Phosphorylated (i.e. activated) S6 protein levels as measured by intra-cellular flow cytometry (MFI - mean fluorescence intensity) in negative control *sgControl*, *sgNprl3* and *sgDepdc5 Eμ-Myc;Cas9* lymphoma cell lines at steady state. n = 2-3 lymphoma cell lines per genotype across three replicate experiments. Non-parametric Kruskal-Wallis test and uncorrected Dunn's test, $^{**}P = 0.0021$, $^{****}P < 0.0001$, 'ns' = not significant. **B**, The *sgNprl3* and *sgDepdc5 Eμ-Myc;Cas9* lymphoma cell lines have elevated expression of genes involved in mTORC1 regulated metabolic pathways compared to the *sgControl Eμ-Myc;Cas9* lymphoma cell lines. Heatmaps show gene expression of mTORC1 regulated

metabolic pathways, lipid/cholesterol biosynthesis, pentose phosphate pathway and one-carbon metabolism from RNA sequencing analysis of *sgControl* (n = 6), *sgNprl3* (n = 6) and *sgDepdc5* (n = 6) *Eμ-Myc;Cas9* lymphoma cell lines after 1% serum starvation for 24 h. **C**, Relative protein translation was measured in negative control *sgControl*, *sgDepdc5* or *sgNprl3 Eμ-Myc;Cas9* lymphoma cell lines after growing for 24 h under starvation conditions (medium containing only 1% instead of 10% fetal calf serum – FCS, starvation) by incorporation of O-propargyl-puromycin (OPP) using Click-iT Plug Alexa Fluor 647 detected by flow cytometry. n = 6 lymphoma cell lines per genotype, 1-2 technical replicates. Ordinary one-way ANOVA statistical test was used for comparison, $^{*}P < 0.05$, $^{**}P < 0.005$.

mTORC1 inhibition reduces hyperactive mTORC1 signaling in GATOR1-deficient lymphoma cells

Since GATOR1-deficient lymphomas displayed elevated mTORC1 signaling causing aberrant metabolic pathway signaling, we next considered whether mTORC1 inhibition would restore signaling to normal levels. Treatment with the mTORC1 inhibitor, rapamycin, markedly reduced the levels of phosphorylated (i.e. activated) S6 in both NPRL3 and DEPDC5 deficient lymphoma cells, both in full medium and following starvation in medium with either reduced serum (1% FCS) or lacking the amino acids [leucine (leu), methionine (met), arginine (arg)] that are uniquely sensed by the GATOR1 complex (Fig. 5A-C). Elevated phosphorylated S6 in these starvation conditions demonstrates that the loss of GATOR1 function drives constitutive mTORC1 activation, as the lack of amino acids should activate the GATOR1 complex thereby inhibiting mTORC1. The levels of phosphorylated S6 in p53 deficient lymphomas were comparable to control lymphomas in full medium and were unaffected by rapamycin treatment or starvation (1% FCS), suggesting that enhanced mTORC1 activity is not a general feature of in *Eu-Myc* lymphomas that developed in the absence of p53 (Fig. 5D). These results prompted us to explore whether reducing mTORC1 signaling could have functional consequences in GATOR1-deficient *Eμ-Myc* lymphoma cells.

Figure 5

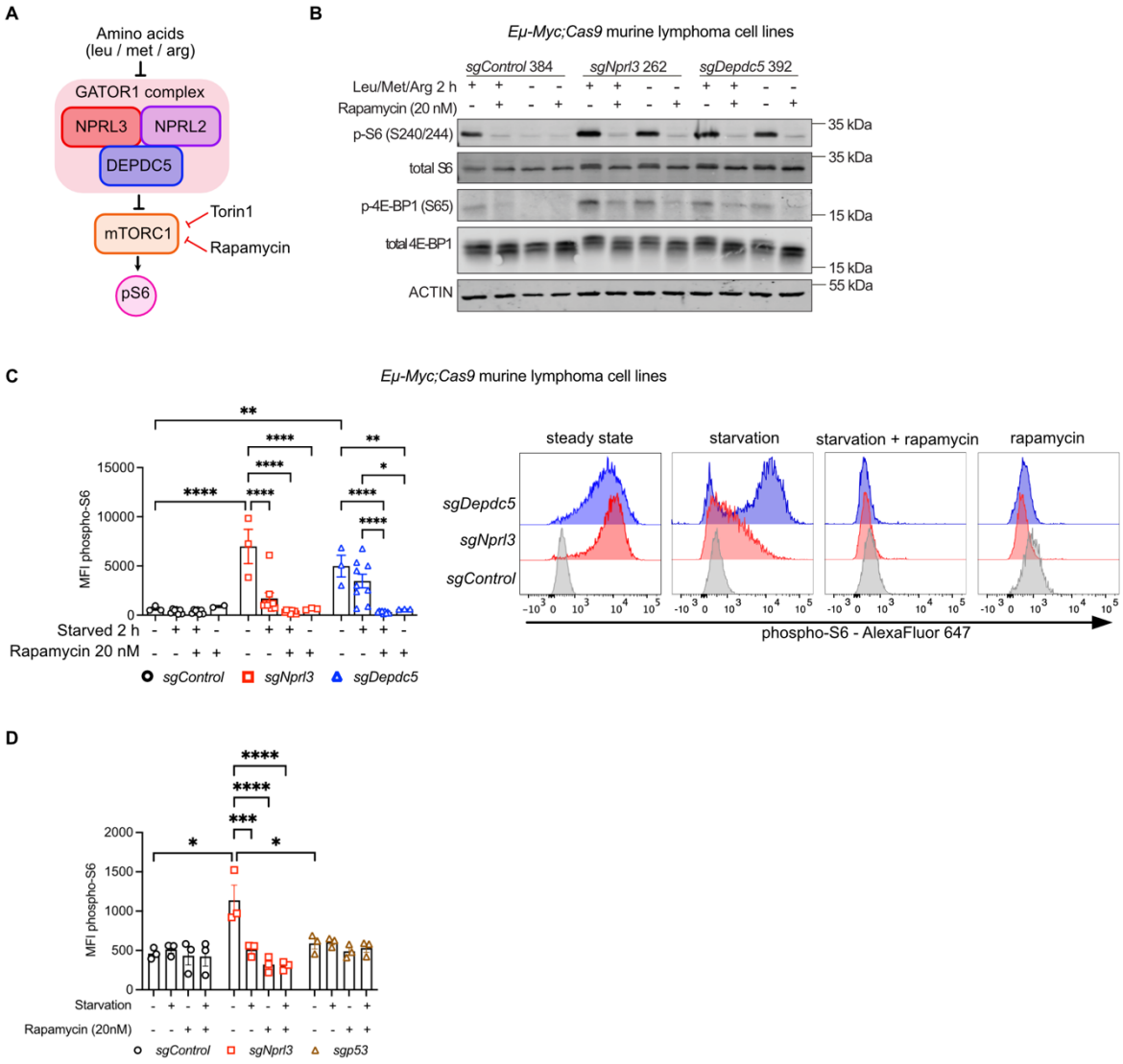

Figure 5. Hyperactive mTORC1 activation in GATOR1-deficient lymphoma cells is reduced to normal levels upon rapamycin treatment.

A, Schematic representation of the GATOR1 complex that negatively regulates mTORC1 signaling in response to deprivation of the amino acids leucine (leu), methionine (met) and arginine (arg). mTORC1 can be directly inhibited by the drug rapamycin or the mTORC1/mTORC2 inhibitor torin1. **B**, Western blot analysis of total S6, phospho-S6 (activated S6), total 4E-BP1 and phospho-4E-BP1 (activated 4E-BP1) proteins in *sgControl*, *sgNprl3* and *sgDepdc5 Eμ-Myc;Cas9* lymphoma cell lines at steady state or after 2 h starvation of the amino acids leucine (leu), methionine (met) and arginine (arg), with and without treatment with rapamycin (20 nM) for 2 h. Blotting for ACTIN served as a protein loading control. Protein sizes are indicated in kDa. **C**, Phospho-S6 (activated S6) protein levels (presented as mean intensity fluorescence – MFI) as measured by intracellular flow cytometry in *sgControl*, *sgNprl3* and *sgDepdc5 Eμ-*

Myc;Cas9 lymphoma cell lines at steady state, steady state plus treatment with rapamycin (20 nM), 2 h starvation (deprived of all amino acids) and 2 h starvation plus treatment with rapamycin (20 nM). Summary graph of phospho-S6 protein levels n = 2-3 lymphoma cell lines per genotype across three replicate experiments are shown on the left and representative FACS histograms, from one representative lymphoma cell line per genotype are shown on the right. **D**, Summary graph of phospho-S6 protein levels in *sgControl*, *sgNprl3* and *sgp53 Eμ-Myc;Cas9* lymphoma cell lines. n = 3 lymphoma cell lines per genotype across one replicate experiment. Data presented as mean ± SEM. 2way ANOVA with Tukey's multiple comparisons test, $^{**}P = 0.0021$, $^{****}P < 0.0001$, 'ns' = not significant.

GATOR1-deficient lymphoma cells are highly sensitive to mTORC1 inhibition

As mTORC1 is constitutively activated in GATOR1-deficient lymphomas, we hypothesized that these cells might be "addicted" to a hyperactive mTORC1 pathway, thereby potentially presenting a therapeutic vulnerability. Of note, rapamycin and torin1 (an inhibitor of both mTORC1 and mTORC2) potently killed GATOR1-deficient but not control or p53-deficient *Eμ-Myc* lymphoma cells *in vitro* (Fig. 6A-B). Remarkably, most RAG1-deficient mice transplanted with GATOR1-deficient lymphomas (lacking either NPRL3 or DEPDC5) could be cured by rapamycin treatment, whereas control lymphomas showed no response, with all recipients presenting with severe malignant disease within 30 days (Fig. 6C-D). These results demonstrate that GATOR1 deficiency causes addiction of lymphoma cells to excess mTORC1 signaling, rendering them vulnerable to mTORC1 inhibitors.

Figure 6

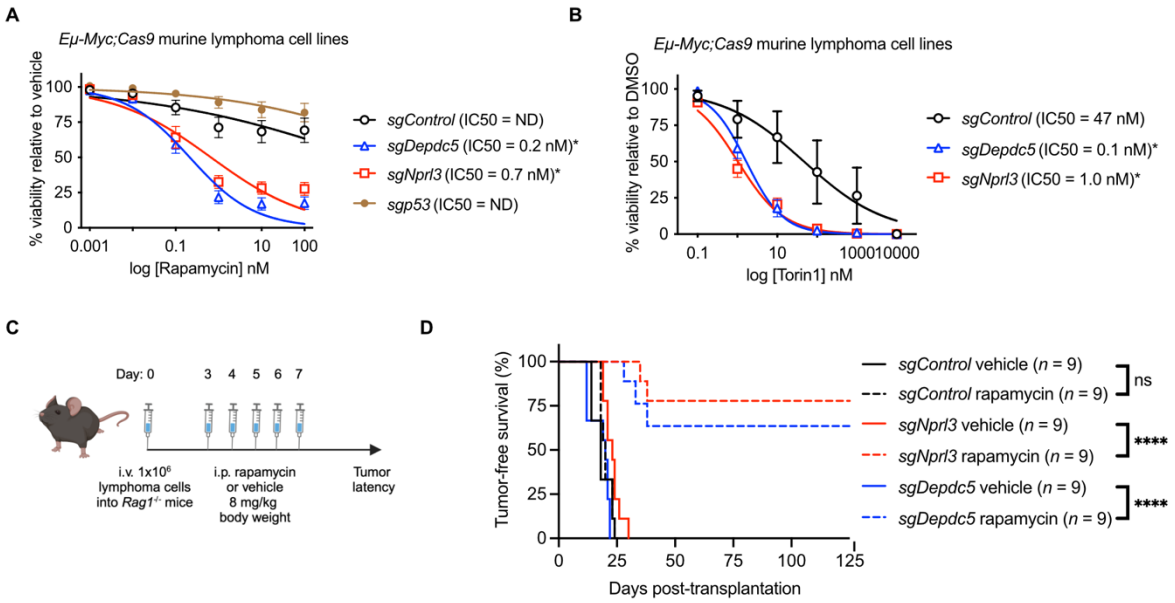

Figure 6. GATOR1-deficient lymphoma cells are highly sensitive to mTORC1 inhibition *in vitro* and *in vivo*.

A-B, Response curves of *sgControl*, *sgNprl3* or *sgDepdc5 Eμ-Myc;Cas9* lymphoma cell lines to treatment with increasing doses of rapamycin **A**, or torin1 **B**. Cell viability was measured after 24 h of treatment with drug or vehicle by staining with AnnexinV plus PI followed by flow cytometric analysis. AnnexinV/PI double negative cells were deemed viable. n = 3-6 cell lines per lymphoma genotype across 3 technical replicates. Data are presented as mean ± SEM, log transformed and fitting to non-linear regression. IC50 values are shown in brackets. Student *t-test* with Welch's correction, $*P < 0.05$. **C**, Schematic of *in vivo* rapamycin treatment experiments. One million *sgControl*, *sgNprl3,* or *sgDepdc5 Eμ-Myc;Cas9* lymphoma cells were transplanted i.v. into the tail vein of RAG1-deficient mice, which lack B and T cells, to prevent lymphoma rejection due to an immune response against Cas9. Two days later, mice were randomly assigned into treatment arms receiving either rapamycin at a dose of 8 mg/kg of body weight for 5 consecutive days by i.p. injection or vehicle as a control. Mice were monitored for lymphoma development. **D**, Tumor-free survival curves of RAG1-deficient mice that had been transplanted with $1x10^6$ negative control *sgControl*, *sgNprl3* or *sgDepdc5 Eμ-Myc;Cas9* lymphoma cell lines. $n = 9$ mice per treatment arm, with three cell lines per sgRNA each injected into three recipient mice. Log-rank (Mantel-Cox) statistical test for survival curve comparison.

Discussion

CRISPR gene knockout screens are a powerful approach to identify critical regulators of biological processes of interest (25,26), such as tumor suppression. While some *in vivo* CRISPR screens have been conducted in mice (27-31), our screen employs primary non-malignant cells (HSPCs from *Eμ-Myc;Cas9* embryos) that can reconstitute the entire blood compartment and give rise to pre-B/B cell lymphomas when transplanted into lethally irradiated recipients. Our investigations demonstrate that genome-wide sgRNA library coverage is maintained *in vivo* as detected in the donor derived non-malignant blood cells present in the recipient mice. Importantly, several hits found in the malignant lymphomas, known and novel candidate tumor suppressors, were identified and validated to suppress MYC-driven lymphomagenesis (32). The success of these screens indicates that this approach can be applied to other biological questions, such as identifying novel suppressors of tumorigenesis driven by different oncogenic lesions, perhaps even in non-hematopoietic cell types, as long as they are amenable to sgRNA library transduction and transplantation into the relevant tissue (e.g. transduction of mammary epithelial stem cells with a sgRNA library followed by their transplantation into cleared mammary fat pads of mice).

Here, by employing the highly efficient CRISPR/Cas9 knockout system in primary HSPCs using an unbiased genome-wide sgRNA library screen, we identify the GATOR1-mTOR axis as one of the most potent tumor suppressive modalities in c-MYC-driven lymphomagenesis, with loss of each of the three GATOR1 components (NPRL3, DEPDC5, NPRL2) having as potent impact as loss of p53 loss. Notably, low levels of GATOR1 are predictive of poorer survival in patients with tumors expressing high levels of *c-MYC*, indicating that this tumor suppressive process may also be critical in diverse types of human cancers.

It has been proposed that adaptation of cellular metabolism is one of the processes engaged by p53 to suppress tumorigenesis (33). However, thus far there are no reports that loss or mutation of such p53 target genes implicated in the control of metabolism can promote tumorigenesis. The explanation for this may be that many genes that are up-regulated in response to p53 activation are not necessarily critical for tumor suppression (34-36). Of note, to recapitulate the spontaneous cancer development caused by loss of p53 (37,38), several p53 target genes, such as the combination of *Puma*, *p21* and *Zmat3* must all be inactivated simultaneously (39,40), due to the extensive redundancy for tumor suppression provided by the diverse cellular responses that can be activated by p53. We hypothesized that p53 may transcriptionally regulate the GATOR1 complex, but our studies using mice with a mutation in the p53 binding site identified in the *Nprl3* promoter favor the notion that p53 and GATOR1 function in distinct processes for tumor suppression.

Importantly, our work revealed that enhanced lymphomagenesis driven by defects in the GATOR1 complex can render such tumor cells abnormally sensitive to mTORC1 inhibitors, highlighting a precision-medicine opportunity for the rational and selective use of such agents in the clinic. Since mTOR inhibitors are already undergoing clinical trials (41), this finding from our work could be rapidly translated.

Methods

Lentiviral constructs and sgRNAs

A positive control sgRNA targeting *p53* (5'-GGCAACTATGGCTTCCACCT); and a negative control sgRNA targeting human-*BIM* (5'-GCCCAAGAGTTGCGGCGTAT) were derived from the constitutive sgRNA FUGW expression vector previously described (40). The genome-wide mouse lentiviral CRISPR sgRNA library used for *in vivo* screening experiments, YUSA v1, was a gift from Kosuke Yusa (Addgene #50947) (11). Two independent sgRNAs for *in vivo* validation experiments of hits and a negative control sgRNA targeting human *NLRC5,* (Supplementary Table 2) were obtained from the Merck CRISPR glycerol stock arrayed mouse sgRNA library available at WEHI (Sigma Aldrich #MSANGERG).

Lentivirus production

Lentiviruses were produced by transient transfection of HEK293T cells in 10 cm^2 dishes with 10 µg of vector DNA and packaging lentiviral constructs pMDL (5 µg), RSV (2.5 µg), and pENV (5 µg) by the standard calcium phosphate precipitation method previously described (42). Viral supernatants were collected 48-72 h after transfection and passed through a 0.45 mM filter prior to transduction of cells.

Animal husbandry and generation of mouse models

The care and use of experimental mice were conducted according to The Walter and Eliza Hall Institute WEHI) Animal Ethics Committee guidelines. C57BL/6-Ly5.2, C57BL/6-Ly5.1 and *Rag1*/J knockout mice were obtained from the WEHI breeding facility (Kew, Victoria, Australia). *Eμ-Myc* transgenic (9), constitutive *Cas9-eGFP* transgenic mice (a gift from Prof K.Rajewsky) (43), and *p53*$^{-/-}$ (38) mice were maintained on a C57BL/6-Ly5.2 background. *Nprl3*-IRES-citrine reporter mice and *Nprl3* promoter p53 binding site mutant mice (denoted NPM mice) were engineered on a C57BL/6 background using CRISPR technology as previously described (44) and further backcrossed with C57BL/6 mice for at least 3 generations prior to use in experiments. The p53 binding site in the promoter of *Nprl3* was identified from previously published ChIPseq data (20). P53 binds to the mouse *Nprl3* promoter at chr11:32167700 to the sequence 'CATGCCCGGACAGG'. The PROMO transcription factor tool was employed to identify other transcription factors that can bind within this sequence and 5 bp upstream and downstream. One transcription factor had overlapping binding in the first and last base of the p53 binding site. Therefore, to impair only p53 binding to the promoter of *Nprl3* while not impacting the binding of other transcription factors, the following precise mutations were made: the first four bases CATG to CCGA and the last four bases were changed from CAGG to AGTG.

Hematopoietic reconstitution of lethally irradiated recipient mice

Embryonic day E13.5 fetal liver cells, a rich source of HSPCs, were collected from *Eμ-Myc*;*Cas9* doubly transgenic mice (both transgenes in a heterozygous state in all experiments) or *p53*$^{+/-}$*;Eμ-Myc*;*Cas9* mice, both on a C57BL/6-Ly5.2 background, and frozen in 90% fetal calf serum (FCS)/10% DMSO (v/v). Fetal liver cells were thawed and cultured in alpha-minimum essential medium (α-MEM) GlutaMAX (Gibco, 35050061) supplemented with 10% FCS (Gibco), 1 mM L-glutamine (Gibco, 25030149), 1 mM sodium pyruvate (Gibco, 11360070), 100 U/mL penicillin-100 μg/mL streptomycin (Gibco, 15140122), 10 mM HEPES (Gibco, 15630080), 50 μM β-mercapto-ethanol and recombinant cytokines (see below) for 48 h prior to lentiviral transduction. The cytokines IL-6 (10 ng/mL), mouse stem cell factor (100 ng/mL), thrombopoietin (50 ng/mL) and FLT-3 ligand (10 ng/mL) were kindly provided by Dr. Jian-Guo Zhang (WEHI). Lentivirus supernatant was generated as described above. Twelve-well non-tissue culture treated plates (Nunc) were coated overnight with retronectin solution (32 μg/mL in PBS, WEHI) at 4°C followed by blocking with 2% bovine serum albumin solution (Sigma-Aldrich, #A1595) in PBS at 37°C for 30 min prior to coating with viral supernatant. Viral particles supplemented with 8 μg/mL polybrene and were centrifuged onto the retronectin coated plates at 3,500 rpm for 2 h. Supernatant was removed from the lentivirus coated plates and fetal liver cells/HSPCs were then added to wells and incubated for 24 h. Transduction efficiency was routinely ~20-30%. Fetal liver cells transduced with vectors encoding sgRNAs were collected and pooled per sgRNA, washed in PBS, filtered through 100 μM mesh, and then injected into lethally irradiated (two doses of 5.5 Gy, 4 h apart) 7-8 week-old C57BL/6-Ly5.1 recipient mice. One fetal liver equivalent was injected into two recipient mice each (~2-3x10^6 cells per recipient mouse). Tumor-free survival was defined as the time from transplantation to ethical endpoint, which was determined by an experienced animal research technician who was blinded to the nature of the injected cells. At sacrifice, peripheral blood was collected and analyzed using an ADVIA hematology analyzer (Bayer) and hematopoietic tissues (spleen, lymph nodes, thymus, bone marrow) were collected for downstream analysis. The pooled CRISPR screens represent 6 independent cohorts. Validation experiments represent 2 independent cohorts. Each hematopoietic reconstitution experiment had internal controls of the same pool of fetal liver cells/HSPCs transduced with a negative control sgRNA (*sgControl*) to account for generational differences in the *Eμ-Myc* mouse colony and possible differences in hematopoietic reconstitution of lethally irradiated recipients between different experiments.

Lymphoma cell transplantation and *in vivo* drug treatment

For *in vivo* drug treatment, 1x10^6 *Eμ-Myc* lymphoma (C57BL/6-Ly5.2) cells resuspended in 200 μL sterile PBS were injected into 7-12 week-old sex-matched recipient *Rag1*$^{-/-}$ mice by intravenous (i.v.) tail vein injection. *Rag1*$^{-/-}$ mice were used as recipient to prevent rejection of lymphoma cells owing to an immune

response to Cas9. After three days, mice were treated for five consecutive days with vehicle or 8 mg/kg body weight rapamycin (LC laboratories) by intra-peritoneal (i.p.) injection. Rapamycin was first dissolved in 100% ethanol, stored at -20°C and further diluted in vehicle, 5.2% PEG 400 and 5.2% Tween 80, immediately before use. Mouse survival time was defined as the time from lymphoma cell line injection until mice were sick and had to be euthanized according to our animal ethics guidelines. This was judged by an experienced animal technician who was blinded to the nature of the lymphoma cells that had been injected and the treatment of the mice.

Genotyping

Mouse genotypes were determined by PCR analysis of DNA derived from earclips or embryonic tails using direct tail lysis buffer (Viagen Biotech) and Proteinase K. Mastermix was prepared with GoTaq green (Promega, M7123) containing primers (final concentration 0.5 pmol/mL) with the addition of 1 mL total DNA. PCR cycling conditions were: 94°C 4 min followed by 30 cycles (94°C for 40 sec, 55°C for 30 sec, 72°C for 60 sec) and finally 72°C for 5 min. PCR products were separated by gel electrophoresis on 2% DNA grade agarose (Bioline) gels in TAE buffer (40 mM Tris Acetate, 1 mM EDTA pH 8.0) containing ethidium bromide (0.2 mg/mL, Sigma) and imaged on GelDoc DOCTM XR+ Gel Documentation system (Bio-Rad). PCR oligonucleotide primers (Integrated DNA Technologies) and expected products were as follows:

Eμ-Myc: expected band size ~900 bp

myc-1: 5' -CAGCTGGCGTAATAGCGAAGAG

myc-2: 5' -CTGTGACTGGTGAGTACTCAACC

***Nprl3*-IRES-citrine:** expected band size of knock-in ~450 bp

Nprl3-FWD: 5' - AGTTTGCAGACTCACCCACC

Nprl3-REV: 5' - TTTCCGCAGAGGGGAAAGAC

***Cas9-eGFP*:** expected band size of knockin ~112 bp and WT ~196 bp

R26F2: 5'- GCCTCCTGGCTTCTGAGGACCG

R26R2: 5'- TCTGTGGGAAGTCTTGTCCCTCC

SAR: 5'-CCTGGACTACTGCGCCCTACAGA

***p53*$^{-/-}$:** expected band size of knockout ~600 bp and WT ~450 bp

P53x6s: 5' -TTATGAGCCACCCGAGGT

P53x7as: 5' - TATACTCAGAGCCGGCCT

Neo18.5: 5' – TCCTCGTGCTTTACGGTATC

Next generation sequencing

To identify pooled CRISPR sgRNAs, genomic DNA was isolated from spleens of reconstituted lymphoma bearing mice (containing malignant and normal hematopoietic cells) using DNeasy Blood and Tissue Kit (Qiagen) according to the manufacturer's instructions. Integrated sgRNAs in each lymphoma sample were amplified from 100 ng of genomic DNA using GoTaq Green Master Mix (Promega) and indexing primers with unique overhangs (12). Amplicons were pooled, cleaned up using Ampure XP beads (Beckman Coulter) and sequenced on Illumina Nextseq or Miseq platform. Enriched sgRNAs per lymphoma were calculated by number of reads mapping to each sgRNA in the library as a proportion of the total number of reads within this lymphoma sample. To identify InDels or mutations in individual target genes, DNA was extracted from lymphoma derived cell lines as described above and PCR amplified using sgRNA specific primers (Supplementary Table 3, *p53* primers as previously described (13) and GoTaq Green Master Mix (Promega). PCR products were amplified a second time using indexing primers, pooled, purified using Ampure XP beads (Beckman Coulter) and sequenced on an Illumina Miseq platform. Reads were aligned to WT reference sequences obtained from Ensembl.

Cell culture

HEK293T cells were cultured in DMEM medium supplemented with 10% FCS. Prior to virus production, HEK293Ts were cultured in DME Glutamax medium (Gibco) supplemented with 10% FCS and 25 mM HEPES. *Eμ-Myc* lymphoma cell lines derived from tumors of sick mice were maintained in FMA medium as previously described (45). Human DoHH2 cells (kindly gifted from Prof David Huang, WEHI, Australia) were cultured in RPMI-1640 medium supplemented with 10% FCS. Human BL2 cells (kindly gifted from Prof Alan Rickinson, The University of Birmingham, UK) were cultured in RPMI-1640 medium supplemented with 10% FCS, 50 μM ∂-thioglycerol (Sigma-Aldrich, M-6145), 1 mM sodium pyruvate (Gibco, 11360070), 2 mM L-glutamine (Gibco, 25030081). *HoxA9-Meis1* murine AML cell lines were cultured in IMDM medium (Gibco, 12440053) supplemented with 10% FCS and IL-3 (100 U/mL; generated in house). All cell lines were regularly verified as mycoplasma negative (MycoAlert mycoplasma detection kit; Lonza, LT07-118) and authenticated by STR profiling at the Australian Genome Research Facility.

***In vitro* drug treatment assays**

To assess drug sensitivity of *Eμ-Myc* lymphoma cells, 5 x 10^4 cells were plated in triplicate into 96-well flat-bottom plates. Cells were treated with rapamycin (Cell Signaling Technology, 9904), torin1 (Cell Signaling Technology, 14379), nutlin-3a (Cayman Chemical, 18585), etoposide (Ebewe Pharmaceuticals Ltd, A-4866) or the MCL-1 inhibitor S63845 (Active Biochem, 6044) at the indicated concentrations. Cell

viability was assessed after 24 h of treatment by staining cells with 2 µg/mL propidium iodide (PI) and AnnexinV conjugated to Alexa Fluor 647 (produced in-house) followed by flow cytometric analysis using a Fortessax20 flow cytometer (Becton Dickinson), 10,000 events were recorded per sample. Data were analyzed using FlowJo analysis software. Cell viability was normalized to control cells treated with an equivalent volume of vehicle, either dimethyl sulfide (DMSO), water or 100% ethanol.

Intracellular flow cytometric analysis for phosphorylated S6

To assess the levels of phosphorylated (i.e. activated) S6 by flow cytometry, lymphoma cells were washed in PBS then resuspended in either FMA medium or Hanks Balanced Salt Solution (HBSS), for starvation condition, without or with supplementation with 20 nM rapamycin and incubated for 2 h at 37ºC in 10% CO_2. Cells were spun down and $1x10^5$ cells were harvested, washed in PBS and stained with green fixable viability dye (Thermo Fisher Scientific). Cells were fixed for 1 h using the eBioscience™ Foxp3/Transcription Factor Staining Buffer Set (Thermo Fisher Scientific) and stained according to the manufacturer's instructions. The antibodies used were directed against phospho-S6 (i.e. activated S6) conjugated to Alexa Fluor 647 (Cell Signaling Technology, 4851). Cells were then analyzed on an LSR IIC flow cytometer (Becton Dickinson). Data were analyzed using FlowJo analysis software and are presented as geometric mean fluorescence intensity (MFI).

Flow cytometric analysis

Immunophenotyping of lymphoma cells was performed on single cell suspensions of primary lymphoma tissue from sick mice or *Eμ-Myc;Cas9* lymphoma derived cell lines stained with fluorochrome-conjugated antibodies against B220 (RA3-6B2), IgM (5.1), IgD (11-26C), T cell antigen receptor beta (TCRβ, H57-597) and CD19 (ID3) in PBS supplemented with 5% FCS and Fcγ receptor block (2.4G2 hybridoma supernatant, WEHI). Donor derived cells were identified as CAS9, i.e. eGFP positive and sgRNA, i.e. CFP or BFP positive. Propidium iodide (PI), final concentration of 2 mg/mL, was used for excluding dead cells during analysis on a Fortessax20 flow cytometer (Becton Dickinson). *Nprl3*-IRES-citrine reporter expression in untreated or drug treated *Nprl3*-IRES-citrine;*Eμ-Myc* lymphoma cell lines was measured using an Aurora1 analyzer (Cytek).

Seahorse mito stress test

Three of each *sgControl, sgNprl3* and *sgDepdc5 Eμ-Myc;Cas9* lymphoma cell lines were treated with 0.45 nM of rapamycin or vehicle (DMSO) for 3 h. Drug was then washed out and $1x10^5$ cells plated in 5 replicate wells for immediate analysis using the Mito Stress Test Kit (Agilent, 103015-100) according to the manufacturer's instructions and using the following drug concentrations: 1.5 µM oligomycin, 2.0 µM

FCCP, 0.5 μM Rotenone/Antimycin A. Mitochondrial function was analyzed on the Seahorse XFe96 (Agilent) analyzer. Plots were prepared using GraphPad Prism software.

Western blotting

Total protein extracts were prepared from *Eμ-Myc;Cas9* lymphoma cell lines and primary lymphomas containing the indicated sgRNAs by lysis in RIPA buffer (50 mM Tris-HCl, 150 mM NaCl, 1% NP-40, 0.5% DOC, 0.1% SDS) containing complete protease inhibitor cocktail (Roche) and phosphatase inhibitor cocktail (PhosphoSTOP^{TM}, Roche). Protein concentration was quantitated by using the Bradford assay (Bio-Rad). Between 10 to 30 μg of protein were prepared in Laemmli buffer boiled for 5 min and proteins size separated by SDS-PAGE using NuPAGE 10% Bis-Tris 1.5 mm gels (Life Technologies). Proteins were then transferred onto nitrocellulose membranes (Life Technologies) using the iBlot membrane transfer system (Thermo Fisher Scientific). Membranes were incubated with the primary antibodies and then the HRP-conjugated secondary antibodies detailed in the Supplementary Table 4, diluted in PBS containing 10% bovine serum albumin with 0.1% Tween20. Luminata Forte Western horseradish peroxidase (HRP) substrate (Merck Millipore) was used for developing the signal and membranes were imaged and analyzed using the ChemiDoc Imaging System with ImageLab software (Bio-Rad). Cell lysates from the p53 mutant *Eμ-Myc* lymphoma cell line (EMRK1172) (23) served as positive control and the p53 wild-type *Eμ-Myc* lymphoma cell line (EMRK1184) (46) served as a negative control for high levels of mutant p53 protein and p19^{ARF} protein. For Western blot detection of phosphorylated proteins, lymphoma cell lines were cultured for 2 h in FMA medium supplemented with 10% dialyzed heat-inactivated FBS, or FMA medium lacking the amino acids leucine, methionine and arginine, supplemented with 10% dialyzed heat-inactivated FBS. Concurrently, these cells were treated with DMSO (vehicle) or 20 nM rapamycin (Cayman Chemical, 20022). Cells were washed with PBS and lysed in ice-cold RIPA buffer containing a protease inhibitor cocktail (Sigma-Aldrich, P8340) and phosphatase inhibitors (PhosSTOP, Roche, 4906837001). Lysates were resolved by SDS-PAGE and transferred onto a nitrocellulose membrane (see above) followed by immunoblotting. Membranes were probed with primary antibodies (see Supplementary Table 4) followed by IRDye secondary antibodies (LI-COR Biosciences, goat anti-rabbit IgG,1:20000, 926-32211 and goat anti-mouse IgG, 1:50000, 926-68070). Membranes were developed using infrared imaging (LI-COR Odyssey CLx).

qRT-PCR analysis

To assess expression of p53 target genes, we used three isogenic *p53* WT or *p53* KO *Eμ-Myc* lymphoma cell lines, a isogenic *p53* WT or *p53* KO *HoxA9-Meis1* AML cell line and isogenic p53 WT or p53 KO human DoHH2 and BL2 cell lines. The p53 KO derivatives were generated by CRISPR/Ca9 as previously

described (12). 1 x 10^6 cells were plated in their respective medium (see above) supplemented with 25 µM Q-VD-OPH (broad spectrum caspase inhibitor, MP Biomedicals) and after 30 min incubation, etoposide (1 µg/mL) or an equal volume of DMSO (vehicle) was added and cells were harvested at 6 h of treatment for gene expression analysis. Total RNA was extracted using Trizol (Thermo Fisher Scientific) and complementary DNA was synthesized using SuperScript First Strand Synthesis SuperMix (Thermo Fisher Scientific), according to the respective manufacturer's instructions. Quantitative reverse-transcription polymerase chain reaction (qRT-PCR) analysis was performed by using the ViiA7 or QuantStudio Real-time PCR system (Thermo Fisher Scientific) using TaqMan Gene Expression Assays (Applied Biosystems) in triplicate as detailed in the Supplementary Table 5. Data were analyzed using QuantStudio software (Thermo Fisher Scientific). Messenger RNA (mRNA) levels were normalized to the expression of the housekeeping gene *Hmbs/HMBS*. All qRT-PCR data were analyzed using $2^{-\Delta\Delta CT}$ method and are presented as fold induction of drug treated cells relative to vehicle treated control cells.

RNA sequencing

Lymphoma cells were cultured in FMA medium containing full serum (10% FCS) or under starvation conditions (FMA medium containing only 1% FCS) for 24 h prior to harvesting. RNA was isolated from *Eμ-Myc* lymphoma cells using a NucleoSpin RNA kit (Macherey-Nagel) following the manufacturer's instructions. The 3' libraries were sequenced with an Illumina NextSeq 500, with single-end 75 bp reads to a depth of 15 M reads per sample. FastQ files were trimmed using Cutadapt (v1.16) and mapped to the mouse reference genome (mm10 GRCm38) using HISAT2 (v2.1.0). Samtools (v1.4.1) was used to convert SAM files to BAM format and to sort BAM files. Counts were generated using featureCounts (v1.6.0). Filtering and normalization of data were carried out using edgeR (v3.16) (47) and differential gene expression analysis was carried out using limma-voom (v3.4.6) (48). Heatmaps were generated using pheatmap (v1.0.12).

Puromycin incorporation assay to determine rate of translation

A previously described protocol, with minor modifications, was employed (49). *Eμ-Myc* lymphoma cells grown in 6-well plates were spiked with 20 µM O-propargyl-puromycin (Thermo Fisher Scientific, C10459) for the final 30 min of the experimental period. Cells were pelleted and washed with PBS. Cells were then fixed with 3.7% paraformaldehyde for 20 min, followed by a 20 min permeabilization with 0.5% Triton-X. Cells were stained using the Click-iTTM Plus Alexa FluorTM 647 Picolyl Azide Toolkit (Thermo Fisher Scientific, C10643) according to the manufacturer's instructions. Puromycin incorporation was analyzed using a LSR FortessaTM X-20 flow cytometer (BD Biosciences).

Lipogenesis assay

A previously described protocol, with minor modifications, was employed (50). Briefly, *Eμ-Myc* lymphoma cells grown in 6-well plates were spiked with 0.2 μCi/mL [1-^{14}C]-acetate (PerkinElmer; NEC084H001MC) for the final 4 h of the experimental period. Cells were pelleted and washed twice with PBS, before lysis in 150 μL 0.5% Triton X-100. Lipids were extracted with 500 μL 2:1 (v/v) chloroform/methanol followed by centrifugation at 1000 rpm for 20 min. 150 μL ^{14}C-labelled lipids from the denser organic fraction were combined with 4 mL OptiPhase HiSafe 3 liquid scintillation cocktail (PerkinElmer; 1200.437) and radio-labeling was quantified using a Tri-Carb 2910 TR Liquid Scintillation Analyzer (PerkinElmer). ^{14}C-acetate incorporation was normalized to cell number.

Identification of p53 binding sites in the *Nprl3* gene locus from published ChIP-seq data

The p53 ChIP-seq data generated in a study from Tonelli et al (20) [PMID: 26372730] were downloaded from GEO database (GSM1828855, GSM1828856, GSM1828857 and GSM1828858). These data include a γ-irradiated B lymphocyte sample (γ-irradiation causes p53 activation), a γ-irradiated non-B lymphocyte sample, a mock treated B lymphocyte sample and a mock treated non-B lymphocyte sample (all cells from mice). ChIP-seq reads were mapped to the MGSCv37/mm9 reference mouse genome using the Subread aligner [PMID: 23558742, 30783653]. Only uniquely mapped reads were retained. Read mapping results were provided to the Homer program [PMID: 20513432] for peak calling. The p53 binding peaks were called for γ-irradiated B lymphocyte and non-B lymphocyte samples separately using an FDR cut-off of 1e-3, with the corresponding mock treated samples as control. Consensus binding motif sequences and corresponding position weight matrices (PWMs) were also obtained from Homer, based on the analysis of genomic sequences found within called peaks. The PWM contains the frequency of each nucleotide type (A, T, G and C) at each location of an enriched motif. The most enriched consensus motif sequence found for the two g-irradiated samples was a p53 binding motif (CATGnnnnnnCATG). We then ran Homer with the p53 PWM to search for exact binding sites of p53 in the called peaks. The p53 binding regions in the gene promoters were defined as a region including a 5 kb upstream sequence and a 2 kb downstream sequence relative to the transcriptional start site of the gene. The RefSeq mouse gene annotation (build 37.2) was used for this analysis.

CUT and RUN assay

The CUT and RUN assay was performed using CUTANA™ CUT and RUN Assays kit (Epicypher, v2.0) following the manufacturer's instructions. Briefly, *Eμ-Myc* lymphoma cell lines used for CUT and RUN assays were pre-treated with 25 μM of the broad-spectrum caspase inhibitor Q-VD-OPH for 45 min and then treated with DMSO or 1 μg/mL etoposide for 6 h. Nuclei were extracted from treated cells and 500,000

nuclei used for each reaction. IgG (0.5 µg) provided with the kit or 1 µL p53 antibody (CM5, Leica Biosystems) were used for immunoprecipitation. NEBNext® Ultra™ II DNA Library Prep Kit for Illumina® (New England Biolabs) and Multiplex Oligos for Illumina Systems (Cell Signaling) were used for library preparation following the manufacturer's instructions. PCR products were purified by using AMPure XP beads (Beckman Coulter). CUT&RUN Libraries were sequenced on a NextSeq 2000, aiming for >$5x10^6$ 60 bp paired end reads per library. Adaptors were trimmed and low-quality reads removed via Trim Galore (The Babraham Institute). Reads were mapped using Bowtie2 (51) with the following settings: *--local--very-sensitive-local --no-unal --no-mixed --no-discordant --phred33 -I 20 -X 2000*. Following conversion of sam files into bam format, duplicate reads were removed with picard-tools, and indexed with samtools (52). Track files were visualised in IGV (53).

Mutational co-occurrence analysis in human DLBCL

Data pertaining to mutations in *p53*, *DEPDC5* and *NPRL2* in human DLBCL samples were obtained from (54-56) and the TCGA database (https://www.cancer.gov/tcga). Waterfall plots were generated for the samples (n = 73) using the waterfall function of the GenVisR (57) R package. Fisher's exact test was used to test for significance of co-occurrence of mutations.

Human Burkitt lymphoma analysis

Gene expression profiles and clinical characteristics were obtained from Lacy et al (58). Human Burkitt lymphoma samples (n = 83) were selected for patient survival analysis. The gene expression levels for *NPRL2*, *NPRL3* and *DEPDC5* across samples were divided into quartiles. Samples were divided into quartiles by *GATOR1*-low group, defined as patients with *NPRL2*, *NPRL3*, or *DEPDC5* expression in the bottom quartile. Otherwise, the sample is designated as *GATOR1*-high. The Kaplan-Meier method was used to estimate the survival functions among patient groups, and the log-rank test was used to test the differences in the overall survival between the selected groups computed using the survminer R package (v0.4.9).

Human TCGA pan-cancer analysis

TCGA pan-cancer RSEM (59) batch normalized mRNA expression data for cancers from patients with expression values for *MYC*, *NPRL2*, *DEPDC5* and *NPRL3* was downloaded from the cBioPortal (n = 10 967 samples) (60,61) on July 30th, 2021. The R statistical software (v4.1.2) was used to conduct patient survival analysis. The Kaplan-Meier survival statistics were computed using R package 'survival' (v3.2-13) and plotted using R package 'survminer' (v0.4.9). Clinical data relating to tumor entity or treatment grade were not available across all cancers. Therefore, further analysis was conducted with all factors present across all samples. Patient samples were first stratified on *MYC*-high expression, defined as samples

where *MYC* expression was higher than the median expression of all samples (n = 5035). Then samples were divided by GATOR1 component expression into quartiles and patient survival was compared between the *GATOR1-low* group defined as tumors with *NPRL2* or *DEPDC5* or *NPRL3* expression in the bottom quartile versus the *GATOR1-high* group defined as *NPRL2* and *DEPDC5* and *NPRL3* expression in the top quartile.

Statistical analysis

GraphPad Prism software (v8) was used to plot Kaplan-Meier mouse survival curves. For comparing two groups, Student's *t*-test was used, and for comparing more than two groups multiple t-test or two-way ANOVA were performed, unless otherwise stated in the figure legends. Data are presented as mean ± standard error of the mean (SEM), unless otherwise stated in figure legends. Significance is deemed where P value is less than 0.05, ns = no significant difference. For the exploratory analysis of the sgRNA counts, heatmaps and pie charts were plotted using R package 'ggplot' (v2_3.3.5), 'o' represents the number of observations of sgRNAs or genes.

References

1. Villunger A, Michalak EM, Coultas L, Mullauer F, Bock G, Ausserlechner MJ*, et al.* p53- and drug-induced apoptotic responses mediated by BH3-only proteins puma and noxa. Science **2003**;302(5647):1036-8 doi 10.1126/science.1090072.
2. Jeffers JR, Parganas E, Lee Y, Yang C, Wang J, Brennan J*, et al.* Puma is an essential mediator of p53-dependent and -independent apoptotic pathways. Cancer Cell **2003**;4(4):321-8 doi 10.1016/s1535-6108(03)00244-7.
3. Nakano K, Vousden KH. PUMA, a novel proapoptotic gene, is induced by p53. Mol Cell **2001**;7(3):683-94 doi 10.1016/s1097-2765(01)00214-3.
4. Yu J, Zhang L, Hwang PM, Kinzler KW, Vogelstein B. PUMA induces the rapid apoptosis of colorectal cancer cells. Mol Cell **2001**;7(3):673-82 doi 10.1016/s1097-2765(01)00213-1.
5. Deng C, Zhang P, Harper JW, Elledge SJ, Leder P. Mice lacking p21CIP1/WAF1 undergo normal development, but are defective in G1 checkpoint control. Cell **1995**;82(4):675-84 doi 10.1016/0092-8674(95)90039-x.
6. Kastenhuber ER, Lowe SW. Putting p53 in Context. Cell **2017**;170(6):1062-78 doi 10.1016/j.cell.2017.08.028.
7. Levine AJ, Momand J, Finlay CA. The p53 tumour suppressor gene. Nature **1991**;351:453-6.
8. Vousden KH, Lane DP. p53 in health and disease. Nat Rev Mol Cell Biol **2007**;8(4):275-83 doi 10.1038/nrm2147.
9. Adams JM, Harris AW, Pinkert CA, Corcoran LM, Alexander WS, Cory S*, et al.* The c-myc oncogene driven by immunoglobulin enhancers induces lymphoid malignancy in transgenic mice. Nature **1985**;318(6046):533-8 doi 10.1038/318533a0.
10. Harris AW, Pinkert CA, Crawford M, Langdon WY, Brinster RL, Adams JM. The E mu-myc transgenic mouse. A model for high-incidence spontaneous lymphoma and leukemia of early B cells. J Exp Med **1988**;167(2):353-71 doi 10.1084/jem.167.2.353.
11. Koike-Yusa H, Li Y, Tan EP, Velasco-Herrera MDC, Yusa K. Genome-wide recessive genetic screening in mammalian cells with a lentiviral CRISPR-guide RNA library. Nature Biotechnology **2014**;32(3):267-73 doi 10.1038/nbt.2800.
12. Aubrey BJ, Kelly GL, Kueh AJ, Brennan MS, O'Connor L, Milla L*, et al.* An inducible lentiviral guide RNA platform enables the identification of tumor-essential genes and tumor-promoting mutations in vivo. Cell Rep **2015**;10(8):1422-32 doi 10.1016/j.celrep.2015.02.002.
13. Aubrey BJ, Janic A, Chen Y, Chang C, Lieschke EC, Diepstraten ST*, et al.* Mutant TRP53 exerts a target gene-selective dominant-negative effect to drive tumor development. Genes Dev **2018**;32(21-22):1420-9 doi 10.1101/gad.314286.118.
14. Pal S, Kaplan JP, Nguyen H, Stopka SA, Savani MR, Regan MS*, et al.* A druggable addiction to de novo pyrimidine biosynthesis in diffuse midline glioma. Cancer Cell **2022**;40(9):957-72.e10 doi https://doi.org/10.1016/j.ccell.2022.07.012.
15. Saxton RA, Sabatini DM. mTOR Signaling in Growth, Metabolism, and Disease. Cell **2017**;168(6):960-76 doi 10.1016/j.cell.2017.02.004.
16. Eischen CM, Weber JD, Roussel MF, Sherr CJ, Cleveland JL. Disruption of the ARF-Mdm2-p53 tumor suppressor pathway in Myc-induced lymphomagenesis. Genes Dev **1999**;13(20):2658-69.
17. Michalak EM, Jansen ES, Happo L, Cragg MS, Tai L, Smyth GK*, et al.* Puma and to a lesser extent Noxa are suppressors of Myc-induced lymphomagenesis. Cell Death Differ **2009**;16(5):684-96.

18. Schmitt CA, McCurrach ME, de Stanchina E, Wallace-Brodeur RR, Lowe SW. *INK4a/ARF* mutations accelerate lymphomagenesis and promote chemoresistance by disabling p53. Genes Dev **1999**;13(20):2670-7.
19. Vassilev LT, Vu BT, Graves B, Carvajal D, Podlaski F, Filipovic Z*, et al.* In vivo activation of the p53 pathway by small-molecule antagonists of MDM2. Science **2004**;303(5659):844-8.
20. Tonelli C, Amati B, Morelli MJ. p53 transcriptional programs in B cells upon exposure to genotoxic stress in vivo: Computational analysis of next-generation sequencing data. Genomics Data **2016**;7:29-31 doi https://doi.org/10.1016/j.gdata.2015.11.006.
21. Kowalczyk MS, Hughes JR, Babbs C, Sanchez-Pulido L, Szumska D, Sharpe JA*, et al.* Nprl3 is required for normal development of the cardiovascular system. Mammalian Genome **2012**;23(7):404-15 doi 10.1007/s00335-012-9398-y.
22. Dutchak Paul A, Laxman S, Estill Sandi J, Wang C, Wang Y, Wang Y*, et al.* Regulation of Hematopoiesis and Methionine Homeostasis by mTORC1 Inhibitor NPRL2. Cell Reports **2015**;12(3):371-9 doi 10.1016/j.celrep.2015.06.042.
23. Wang Z, Hu H, Heitink L, Rogers K, You Y, Tan T*, et al.* The anti-cancer agent APR-246 can activate several programmed cell death processes to kill malignant cells. Cell Death & Differentiation **2023**;30(4):1033-46 doi 10.1038/s41418-023-01122-3.
24. Kotschy A, Szlavik Z, Murray J, Davidson J, Maragno AL, Le Toumelin-Braizat G*, et al.* The MCL1 inhibitor S63845 is tolerable and effective in diverse cancer models. Nature **2016**;538(7626):477-82 doi 10.1038/nature19830.
25. Shalem O, Sanjana NE, Hartenian E, Shi X, Scott DA, Mikkelson T*, et al.* Genome-scale CRISPR-Cas9 knockout screening in human cells. Science **2014**;343(6166):84-7 doi 10.1126/science.1247005.
26. Wang T, Wei JJ, Sabatini DM, Lander ES. Genetic Screens in Human Cells Using the CRISPR-Cas9 System. Science **2014**;343(6166):80-4 doi doi:10.1126/science.1246981.
27. Chow RD, Chen S. Cancer CRISPR Screens In Vivo. Trends Cancer **2018**;4(5):349-58 doi 10.1016/j.trecan.2018.03.002.
28. Dong MB, Wang G, Chow RD, Ye L, Zhu L, Dai X*, et al.* Systematic Immunotherapy Target Discovery Using Genome-Scale In Vivo CRISPR Screens in CD8 T Cells. Cell **2019**;178(5):1189-204.e23 doi 10.1016/j.cell.2019.07.044.
29. Sutra Del Galy A, Menegatti S, Fuentealba J, Lucibello F, Perrin L, Helft J*, et al.* In vivo genome-wide CRISPR screens identify SOCS1 as intrinsic checkpoint of CD4(+) T(H)1 cell response. Sci Immunol **2021**;6(66):eabe8219 doi 10.1126/sciimmunol.abe8219.
30. Wertz MH, Mitchem MR, Pineda SS, Hachigian LJ, Lee H, Lau V*, et al.* Genome-wide In Vivo CNS Screening Identifies Genes that Modify CNS Neuronal Survival and mHTT Toxicity. Neuron **2020**;106(1):76-89.e8 doi 10.1016/j.neuron.2020.01.004.
31. Xu C, Qi X, Du X, Zou H, Gao F, Feng T*, et al.* piggyBac mediates efficient in vivo CRISPR library screening for tumorigenesis in mice. Proceedings of the National Academy of Sciences of the United States of America **2017**;114(4):722-7 doi 10.1073/pnas.1615735114.
32. Pelengaris S, Khan M, Evan G. c-MYC: more than just a matter of life and death. Nat Rev Cancer **2002**;2(10):764-76 doi 10.1038/nrc904.
33. Bensaad K, Tsuruta A, Selak MA, Vidal MNC, Nakano K, Bartrons R*, et al.* TIGAR, a p53-Inducible Regulator of Glycolysis and Apoptosis. Cell **2006**;126(1):107-20 doi https://doi.org/10.1016/j.cell.2006.05.036.
34. Brady CA, Jiang D, Mello SS, Johnson TM, Jarvis LA, Kozak MM*, et al.* Distinct p53 transcriptional programs dictate acute DNA-damage responses and tumor suppression. Cell **2011**;145(4):571-83 doi 10.1016/j.cell.2011.03.035.

35. Li T, Kon N, Jiang L, Tan M, Ludwig T, Zhao Y*, et al.* Tumor suppression in the absence of p53-mediated cell-cycle arrest, apoptosis, and senescence. Cell **2012**;149(6):1269-83 doi 10.1016/j.cell.2012.04.026.
36. Valente LJ, Gray DH, Michalak EM, Pinon-Hofbauer J, Egle A, Scott CL*, et al.* p53 efficiently suppresses tumor development in the complete absence of its cell-cycle inhibitory and proapoptotic effectors p21, Puma, and Noxa. Cell Rep **2013**;3(5):1339-45 doi 10.1016/j.celrep.2013.04.012.
37. Donehower LA, Harvey M, Slagle BL, McArthur MJ, Montgomery CA, Jr., Butel JS*, et al.* Mice deficient for p53 are developmentally normal but susceptible to spontaneous tumours. Nature **1992**;356(6366):215-21 doi 10.1038/356215a0.
38. Jacks T, Remington L, Williams BO, Schmitt EM, Halachmi S, Bronson RT*, et al.* Tumor spectrum analysis in *p53*-mutant mice. Curr Biol **1994**;4(1):1-7.
39. Bieging-Rolett KT, Kaiser AM, Morgens DW, Boutelle AM, Seoane JA, Van Nostrand EL*, et al.* Zmat3 Is a Key Splicing Regulator in the p53 Tumor Suppression Program. Mol Cell **2020**;80(3):452-69 e9 doi 10.1016/j.molcel.2020.10.022.
40. Janic A, Valente LJ, Wakefield MJ, Di Stefano L, Milla L, Wilcox S*, et al.* DNA repair processes are critical mediators of p53-dependent tumor suppression. Nat Med **2018**;24(7):947-53 doi 10.1038/s41591-018-0043-5.
41. Ali ES, Mitra K, Akter S, Ramproshad S, Mondal B, Khan IN*, et al.* Recent advances and limitations of mTOR inhibitors in the treatment of cancer. Cancer Cell International **2022**;22(1):284 doi 10.1186/s12935-022-02706-8.
42. Herold MJ, van den Brandt J, Seibler J, Reichardt HM. Inducible and reversible gene silencing by stable integration of an shRNA-encoding lentivirus in transgenic rats. Proceedings of the National Academy of Sciences of the United States of America **2008**;105(47):18507-12 doi 10.1073/pnas.0806213105.
43. Chu VT, Weber T, Graf R, Sommermann T, Petsch K, Sack U*, et al.* Efficient generation of Rosa26 knock-in mice using CRISPR/Cas9 in C57BL/6 zygotes. BMC Biotechnology **2016**;16(1):4 doi 10.1186/s12896-016-0234-4.
44. Kueh AJ, Pal M, Tai L, Liao Y, Smyth GK, Shi W*, et al.* An update on using CRISPR/Cas9 in the one-cell stage mouse embryo for generating complex mutant alleles. Cell Death Differ **2017**;24(10):1821-2 doi 10.1038/cdd.2017.122.
45. Kelly GL, Grabow S, Glaser SP, Fitzsimmons L, Aubrey BJ, Okamoto T*, et al.* Targeting of MCL-1 kills MYC-driven mouse and human lymphomas even when they bear mutations in p53. Genes Dev **2014**;28(1):58-70 doi 10.1101/gad.232009.113.
46. Baell JB, Leaver DJ, Hermans SJ, Kelly GL, Brennan MS, Downer NL*, et al.* Inhibitors of histone acetyltransferases KAT6A/B induce senescence and arrest tumour growth. Nature **2018**;560(7717):253-7 doi 10.1038/s41586-018-0387-5.
47. Robinson MD, McCarthy DJ, Smyth GK. edgeR: a Bioconductor package for differential expression analysis of digital gene expression data. Bioinformatics **2009**;26(1):139-40 doi 10.1093/bioinformatics/btp616.
48. Ritchie ME, Phipson B, Wu D, Hu Y, Law CW, Shi W*, et al.* limma powers differential expression analyses for RNA-sequencing and microarray studies. Nucleic Acids Res **2015**;43(7):e47 doi 10.1093/nar/gkv007.
49. Pavlova NN, King B, Josselsohn RH, Violante S, Macera VL, Vardhana SA*, et al.* Translation in amino-acid-poor environments is limited by tRNA(Gln) charging. Elife **2020**;9 doi 10.7554/eLife.62307.
50. Ricoult SJ, Yecies JL, Ben-Sahra I, Manning BD. Oncogenic PI3K and K-Ras stimulate de novo lipid synthesis through mTORC1 and SREBP. Oncogene **2016**;35(10):1250-60 doi 10.1038/onc.2015.179.
51. Langmead B, Salzberg SL. Fast gapped-read alignment with Bowtie 2. Nature methods **2012**;9(4):357-9 doi 10.1038/nmeth.1923.

52. Danecek P, Bonfield JK, Liddle J, Marshall J, Ohan V, Pollard MO*, et al.* Twelve years of SAMtools and BCFtools. Gigascience **2021**;10(2) doi 10.1093/gigascience/giab008.
53. Robinson JT, Thorvaldsdottir H, Winckler W, Guttman M, Lander ES, Getz G*, et al.* Integrative genomics viewer. Nature biotechnology **2011**;29(1):24-6 doi 10.1038/nbt.1754.
54. Morin RD, Mendez-Lago M, Mungall AJ, Goya R, Mungall KL, Corbett RD*, et al.* Frequent mutation of histone-modifying genes in non-Hodgkin lymphoma. Nature **2011**;476(7360):298-303 doi 10.1038/nature10351.
55. Lohr JG, Stojanov P, Lawrence MS, Auclair D, Chapuy B, Sougnez C*, et al.* Discovery and prioritization of somatic mutations in diffuse large B-cell lymphoma (DLBCL) by whole-exome sequencing. Proc Natl Acad Sci U S A **2012**;109(10):3879-84 doi 10.1073/pnas.1121343109.
56. Chapuy B, Stewart C, Dunford AJ, Kim J, Kamburov A, Redd RA*, et al.* Molecular subtypes of diffuse large B cell lymphoma are associated with distinct pathogenic mechanisms and outcomes. Nat Med **2018**;24(5):679-90 doi 10.1038/s41591-018-0016-8.
57. Skidmore ZL, Wagner AH, Lesurf R, Campbell KM, Kunisaki J, Griffith OL*, et al.* GenVisR: Genomic Visualizations in R. Bioinformatics **2016**;32(19):3012-4 doi 10.1093/bioinformatics/btw325.
58. Lacy SE, Barrans SL, Beer PA, Painter D, Smith AG, Roman E*, et al.* Targeted sequencing in DLBCL, molecular subtypes, and outcomes: a Haematological Malignancy Research Network report. Blood **2020**;135(20):1759-71 doi 10.1182/blood.2019003535.
59. Li B, Dewey CN. RSEM: accurate transcript quantification from RNA-Seq data with or without a reference genome. BMC Bioinformatics **2011**;12(1):323 doi 10.1186/1471-2105-12-323.
60. Cerami E, Gao J, Dogrusoz U, Gross BE, Sumer SO, Aksoy BA*, et al.* The cBio cancer genomics portal: an open platform for exploring multidimensional cancer genomics data. Cancer Discov **2012**;2(5):401-4 doi 10.1158/2159-8290.Cd-12-0095.
61. Gao J, Aksoy BA, Dogrusoz U, Dresdner G, Gross B, Sumer SO*, et al.* Integrative analysis of complex cancer genomics and clinical profiles using the cBioPortal. Sci Signal **2013**;6(269):pl1 doi 10.1126/scisignal.2004088.

Acknowledgments

The authors thank all members of the Blood Cells and Blood Cancer Division at The Walter and Eliza Hall Institute (WEHI*)*, the Genome Engineering and Cancer Modelling Program at the Olivia Newton-John Cancer Research Institute (ONJCRI) for their support, advice, and sharing of reagents; G Siciliano and other Bioservices staff for technical assistance with the *in vivo* experiments and animal husbandry; A Aeslop and the Screening lab at WEHI for the glycerol stock sgRNAs for target validation. Visual schematics were created using BioRender.com. This work was supported by grants and fellowships from the Australian National Health and Medical Research Council (NHMRC) (Project Grants 1159658,1186575 and 1145728 to MJH, 1143105 to MJH and AS, Ideas Grants 2002618 and 2001201 to GLK, 2004212 and 2012313 to KKB, Program Grant 1113133 to AS and Fellowships 1020363 to AS, 2017971to MJH), the Leukemia and Lymphoma Society of America (LLS SCOR 7015-18 to AS, GLK, MJH), the Cancer Council of Victoria (project grant 1147328 and 2021 Grant In Aid to MJH, 1052309 to AS ,1147328 to GLK and Venture Grant to MJH and AS), Victorian Cancer Agency (MCRF Fellowship 17028 to GLK and 17020 to KKB), Phenomics Australia (to AJK and MJH) the estate of Anthony (Toni) Redstone OAM (AS and GLK), the Craig Perkins Cancer Research Foundation (GLK), the Dyson Bequest (GLK), the Harry Secomb Trust (GLK), the University of Melbourne Research Training scholarship (MAP) and the Uehara Memorial Foundation and JSPS Grant-in-Aid for Research Activity Start-up 20K22854 (SM). The generation of *Nprl3-IRES-citrine* and *Nprl3* promoter mutant mice used in this study was supported by Phenomics Australia and the Australian Government through the National Collaborative Research Infrastructure Strategy (NCRIS) program. This work was made possible by operational infrastructure grants through the Australian Government Independent Research Institute Infrastructure Support Scheme (361646 and 9000220) and the Victorian State Government Operational Infrastructure Support Program.

Author contributions

MJH and AS conceived and designed the study; MAP, SM, YD, GH, ZW, and CK conducted experiments; SV, KET and KKB conducted metabolomic studies and relating analyses; GG and ATP conducted pan-cancer analysis and CRISPR screen library analyses; SS and ADJ conducted survival analyses on human Burkitt lymphoma samples and p53 mutual exclusivity analysis in human DLBCL; YL and WS re-analyzed public ChIP sequencing data and identified p53 binding site in the *Nprl3* promoter to mutate; SW ran NGS; AJK and LT engineered new mouse models; LW provided technical mouse support; GP, AW, DK and SD provided reagents; MM and JEV supported CUT & RUN experiments; MAP, SM, YD, SV, KET, KKB, AS and MJH analyzed and interpreted results; MAP, EJL, MJH and AS drafted and edited the manuscript with additional editing from all authors.

Competing interests

The authors declare no conflicts of interest with respect to this work.

Additional information

Supplementary Figures and information are available for this paper. Correspondence and requests for materials should be addressed to Marco Herold marco.herold@onjcri.org.au